SÜMEYRA İSTENGİR

M.S. Thesis in Physics

August- 2010

INVESTIGATION OF STRUCTURAL and LUMINESCENT CHARACTERIZATION OF WET- ETCHED SILICON

by

Sümeyra İSTENGİR

August 2010

INVESTIGATION OF STRUCTURAL and LUMINESCENT CHARACTERIZATION OF WET- ETCED SILICON

by

Sümeyra İstengir

A thesis submitted to

the Graduate Institute of Sciences and Engineering

of

Fatih University

in partial fulfillment of the requirements for the degree of

Master of Science

in

Physics

August 2010
Istanbul, Turkey

APPROVAL PAGE

I certify that this thesis satisfies all the requirements as a thesis for the degree of Master of Science.

Prof. Dr. Mustafa KUMRU
Head of Department

This is to certify that I have read this thesis and that in my opinion it is fully adequate, in scope and quality, as a thesis for the degree of Master of Science.

Assoc. Prof. Bayram ÜNAL
Supervisor

Examining Committee Members

Assoc. Prof. Bayram ÜNAL ______________________

Assoc. Prof. Abdulhadi BAYKAL ______________________

Assist. Prof. Kurtuluş GÖLCÜK ______________________

It is approved that this thesis has been written in compliance with the formatting rules laid down by the Graduate Institute of Sciences and Engineering.

Assoc. Prof. Nurullah ARSLAN
Director

Date
August 2010

INVESTIGATION OF STRUCTURAL and LUMINESCENT CHARACTERIZATION OF WET-ETCHED SILICON

Sümeyra İSTENGİR

M.S. Thesis – Physics
August 2010

Supervisor: Assoc. Prof. Dr. Bayram ÜNAL

ABSTRACT

In this thesis, visible photoluminecent nanoporous silicon thin film is fabricated by the method of stain etching processes under various surfactants in order to characterize the homogenous luminescent nanostructures at room temperature. For the fist time, a couple of special surfactants has been used for the stain etching technique which prevents to ceasing the etching process, usually addition of some kind of surfactans into etching solution ending most of the etching processes.

Several characterization techniques have been utilized in order to understand the etching mechanism and optical properties of the luminescent porous silicon layers including depth profiles for the first time in the literature. These characterization techniques have also been correlated with the type and content of the surfactants used in this experiment. Optical and structural effects of the surfactants on the nanostructures of porous silicon have been evaluated using a photoluminescence (PL) spectroscopy, photoluminescence excitation (PLE) spectroscopy, x-ray photoelectron (XPS) spectroscopy and confocal scanning laser optical (CSLM) microscopy.

As a conclusion, the characterization techniques mentioned above show that surfactants mainly labeled as PF and RF types used in this study have variety of the deep influences on the speed of etching processes, as well as on optical and the structural properties, of the visible photoluminecent porous silicon.

Keywords: Nanoporous Silicon, Chemical Etching, Surfactants, Photoluminescence, Confocal Microscopy.

KİMYASAL AŞINDIRMALI SİLİSYUMUN YAPISAL VE IŞILDAMALI KARAKTERİSTİĞİNİN İNCELENMESİ

Sümeyra İSTENGİR

Yüksek Lisans Tezi – Fizik
Ağustos 2010

Tez Danışmanı: Doç. Dr. Bayram ÜNAL

ÖZ

Bu çalışmada, oda sıcaklığında, homojen lüminesant nanoyapıları karakterize etmek için, lekeli aşındırma metodu basamaklarında çeşitli surfaktanlar kullanılarak görünür fotoluminesant silisyum ince film üretilmiştir. Lekeli aşındırma metodu için, aşındırma işlemini durduran, genellikle, aşındırma çözeltisi içerine bir çeşit surfaktanların eklenmesi ilk defa kullanılmıştır.

Lüminesent gözenekli silisumyum tabakalarının aşındırma mekanizmasını ve optiksel özelliklerini anlamak için, ilk defa derinlik profillerinide içeren çeşitli karakterizasyon teknikleri kullanılmıştır.

Bu karakterizasyon teknikleri ile deneyde kullanılan surfaktanın tipi ve içeriği ilişkilendirilmiştir. Gözenekli silisyumun nanoyapıların optiksel ve yapısal etkileri Fotolüminesant Spektroskopisi, X-ışını Fotoelektron Spektroskopisi ve Konfokal Lazer Taramalı Mikroskop kullanılarak elde edilmiştir.

Sonuç olarak, yukarıda bahsedilen karakterizasyon teknikleri; bu çalışmada kullanılan başlıca PF ve RF olarak adlandırılan surfaktanların , görünür fotolüminesant gözenekli silisyumun hem optiksel ve yapısal özellliklerinde, hem de aşındırma işlemlerinin hızı üzerindeki derin etkilerinin çeşitliğini göstermektedir.

Anahtar Kelimeler: Nanogözenekli Silisyum, Kimyasal Aşındırma, Yüzey Gerilimini Düşürücü Maddeler (surfaktan), Fotoluminesans, Konfokal Mikroskop.

To my family and all my friends

ACKNOWLEDGEMENT

First of all, I would like to gratitude to my supervisor Assoc. Prof. Dr. Bayram ÜNAL for his help, motivation, stimulating and incentive suggestions during whole time of research and for writing this thesis.

I want to thank to Assist. Prof. Dr. Kurtuluş GÖLCÜK for his stimulation and motivation in my thesis.

My special thanks go to Assist. Prof. Sedat COŞGUN for helping me and making me coping with the chemistry part of this study.

I appreciate my colleague, Mr. Ali KARATUTLU for his valuable contributions during all stages of the experimental work and his endless patient.

I am grateful to Gebze High Institute of Technology (GHIT) to Mr. Ali AHSEN for XPS measurements.

I want to appreciate Assoc. Prof. Abdulhadi BAYKAL for his valuable contributions and great helps related to corrections and ideas about the processes.

I express my thanks and appreciation of my family for their understanding, motivation, supporting and patience.

Finally, I am thankful to all my friends and colleagues motivating and encouraging me to accomplish the study on time.

TABLE OF CONTENTS

LIST OF FIGURES

LIST OF SYMBOLS AND ABBREVIATIONS

LEPSi : Light Emitting PSi

CSLM : Confocal scanning Laser Microscopy

SC : Surface Clean

PL : Photoluminescence

PLE : Photoluminescence Excitation

XPS : X-Ray Photo-electron Spectroscopy

PS : Porous Silicon

CVD : Chemical Vapor Deposition

MBE : Molecular Beam Epitaxy

SOI : Silicon-On-Insulator

QCE : Quantum Confinement Effect

FWHM: Full Width at Half Maximum

LCAO : Linear Combination of Atomic Orbitals

HOMO : Highest Occupied Molecular Orbital

LUMO : Lowest Unoccupied Molecular Orbital

CL : Cathodoluminescence

CMC : Critical Micelle Concentration

BE : Binding energy of photoelectrons

ε : Excitation energy of X-ray source

$\rho_{DOS}(E)$:Density of states per unit energy per unit volume

E-k : Energy-Wave vector

$\psi k(\mathbf{r})$: Wave functions

$g_c(E)$: Density of states at an energy E in the conduction band

$g_v(E)$: Density of states at an energy E in the valence band

f(E) : Fermi-Dirac distribution function

m_c : Effective mass of the electrons in the conduction band

m_v : Effective mass of the holes in the valence band

n : Electron concentration

p : Hole concentration

N_C : Effective density of states in the conduction band

N_V : Effective density of states in the valence band

N_0 : Number of incident photons per second

d : Thickness of the film

h : Quantum efficiency

t : Recombination lifetime

t_1 : Carrier transit time

CHAPTER 1

1. INTRODUCTION

Nanotechnology presents us an understanding and knowledge of how to control matter in nanoscale, between 1 to 100 nm range where many novel properties are discovered and investigate the face of nature in nanoscale. If one likes to know the shortest and most complete definition of nanotechnology one should refer to the statement by the US National Science and Technology Council which states: "The essence of nanotechnology is the ability to work at the molecular level, atom by atom, to create large structures with fundamentally new molecular organization. The aim is to exploit these properties by gaining control of structures and devices at atomic, molecular, and supramolecular levels and to learn to efficiently manufacture and use these devices". In short, nanotechnology is the ability to build micro and macro materials and products with atomic precision.

From the early studies of nanotechnology through the last two decades, there has been numerous contributions of silicon in this field. Silicon has many industrial uses as well. It is the principal component of most semiconductor devices, most importantly integrated circuits or microchips. Silicon is widely used in semiconductors because it remains a semiconductor at higher temperatures than the semiconductor germanium and because its native oxide is easily grown in a furnace and forms a better semiconductor/dielectric interface than any other material. Hence, Silicon has a very important role of macro- and micro-technology towards nanoscale as a core element from its discovery by reducing SiF_4 with potassium in 1824 by Jöns Jacop Berzelius a Swedish chemist, until another century for a deeper understanding of the semiconducting studies, established on the original work of Bethe, Bloch, Braun, Lark-Horovitz, Mott, Pohl, Schottky, Wilson and many others between 1930 and 1940. These works caused finally the invention of the transistor by Bardeen, Brattain and Shockley in 1947. Nevertheless, the first transistor was made from germanium because of the fact that the way is not found to grow silicon until 1950 by crucible pulling.

The discovery of float zone (FZ) method led the first silicon-based transistor formed in 1954 by Teal. The preparation of silicon set up a relation to silane which is one of previous compounds for obtaining elemental silicon by using chemical vapor deposition (CVD) after purifying by distillation and adsorption process. The formation of integrated silicon circuit caused what is known today as Silicon age by Kilby in 1958. [1]

Silicon has been used to several electrochemical researches. Early studies on electrochemistry were related to electropolishing, anodic oxidation, and chemical etching. Guentherschulze and Betz made the first experiments for growing anodic oxides on silicon in the beginning of 1937 [2]. More detailed study has been made by Schmidt and Michel who presented light patterns on the n-type cause local anodic oxidation [3] in 1957 [4]. The dissolution mechanism for silicon electrodes in HF and the formed films to be a consequence of Si from SiF_2 were presented by Meeming and Schwandt in 1966 [5]. In 1970, macropores on n-type substrates and their dependence on crystal orientation were given in a report by Theunissen and co-workers [6]. The first studies on electrochemical etch-stop techniques [7] and photoelectrochemical etching [8] of n-type techniques were made in the same year.

The porous structure of electrochemically formed films on silicon electrodes were firstly demonstrated by Watanabe and Sakai [9] in 1971. This caused a rapid increase in publications related to the electrochemistry of silicon and PS. In 1972, Theunissen [10] made first model of porous silicon by using n-type silicon electrodes and explained the model established on a breakdown of the depletion layer. In 1988, random macropore production in pattern was showed via using n-type silicon electrode [11]. The size of pore diameters might be as small as 2nm which was illustrated Bomchil et 1983 [12]. Watanabe and Sakai reported [10] the conversion of PS to SiO_2 by using thermal oxidation in 1971. Arita made thermal oxidation experiment on PS in 1978 [13] and Unigami's study [14] let researchers to know how to make an silicon-on-insulator (SOI) technology established on oxidized PS [15, 16] in 1980. In 1986, growing a Si molecular beam epitaxy (MBE) film on PS and subsequent oxidation led to develop another way made by Lin and coworkers [17], to manufacturing SOI structures. On the other hand, the main problem of PS-based SOI technologies is that the windows is not necessary in the Si film to accomplish the oxidation of the underlying PS. Pickering and co-workers presented in 1984 [18] that visible photoluminescence (PL) from PS at 4.2 K , that they made an interpretation as due to a complex mixture of amorphous phases. The physical idea behind the light emitting PS, called as LEPSi, kept in the mind of researchers as a question until the outstanding discovery of photoluminescence of porous silicon in room temperature in 1990 by Leigh Canham, a British scientist. An explanation had not been offered until 1990-1991, but proposal of quantum size effect [19, 20]. Oxidized PS has been found two years later [21, 22]. These mysterious optical properties of PS was a reason for growing demand on vigorous research and made more than a thousand publications, as well as several books and reviews [23, 24].

CHAPTER 2

2. SEMICONDUCTORS

2.1 PHYSICS BEHIND SEMICONDUCTOR SILICON

A semiconductor Silicon ingot has gray color, glassy appearance, and face-centered crystal structure. The element takes place in the column IV of the perodic table. The crystal structure of Silicon is the same as diamond has shown in figure 2.1 below [25] :

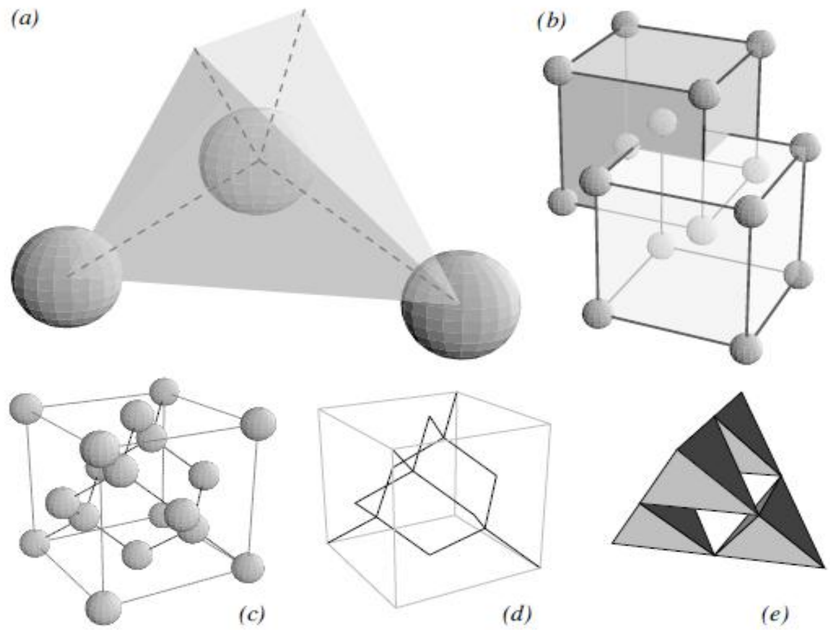

Figure 2.1 The diamond-like structure of the Silicon crystal is made by the tetrahedral arrangement of the four sp^3 bond-forming orbitals of the silicon atom, symbolically shown (a) as stippled lines fastening the ball-like atomic nuclei in this tetrahedral repeating unit. (b) When the atoms combine to create a crystal, we observe a structure that may be viewed as a set of two nested cubic lattices, or (c) a single face-centered cubic lattice with a basis. (d) The structure of the sp^3 hybrid bonds. (e) The fcc unit cell can also be viewed as four tetrahedral.

2.2 FEATURES OF SEMICONDUCTORS

2.2.1 Energy Band Structure of Semiconductors

The band structure is the difference between the lowest position of the valance band and the highest position of conduction band. There is either direct or indirect band structure like Silicon shown in figure 2.2. Furthermore, the band structure defines optical properties of the semiconductor. At temperatures T > 0°K, the optical spectra is broaden and shifted by the agitation (excitation) of thermal lattice vibrations [26].

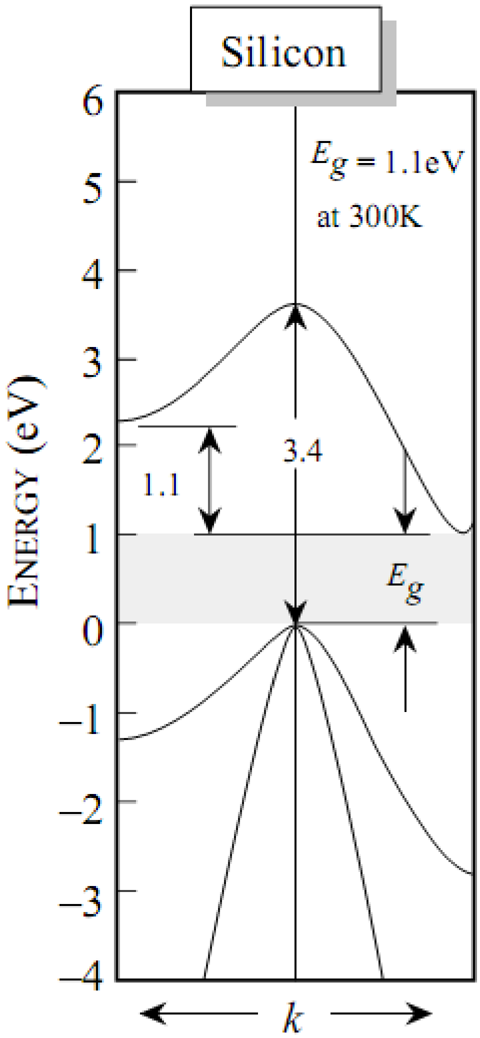

Figure 2.2 Energy-wavevector (E-k) diagram for indirect bandgap elemental semiconductor of silicon [27]

Input parameters which are derived from spectroscopic data are used in calculation of electronic band structures. Practically all significant physical quantities pertaining to semiconductor band structures have been pulled out from empirical spectra of absorption, emission, and reflectivity. The most applicable parameters are basic and higher band gaps, the magnitude of momentum matrix elements, symmetries of wave functions at special points in the Brillouin zone, and the joint density of states of the band structure [26].

2.2.2 Density of States

In a study [28] it is given that the states in the bands and their dependence on energy are defined by the density of states. In the conduction or valance band, carriers are found either localized impurity states or delocalized continuum states. In the most uncopmlicated way, each impurity carries a single, nondegenerate state. Hence, the number of impurity states is the same with the concentration of impurities. The electronic density of states is known as the number of electron states per unit volume per unit energy. As Pauli principle states that only two electrons with opposite spin can occupy one volume element in phase space, the principle causes the finiteness of density states. Here, the phase space is the combination of six-dimensional space which is the summation of three real space and three momentum space. If we define a volume element in the phase space to include a range of positions and momentum of the particle which are distinguishable from the position and momenta of other particles. So as to be different, the limit of the position and momenta must equal or surpass the limit given by the uncertainty relation. The volume element in the phase is then written by

$$\Delta x\,\Delta y\,\Delta z \cdot \Delta p_x \cdot \Delta p_y\,\Delta p_z = (2\pi\hbar)^3 \qquad (2.1)$$

The volume element in phase space is $(2\pi\hbar)^3$. It is familiar for a system with one degree of freedom that the equation (2.1) is written as one-dimensional Heisenberg uncertainty principle $\Delta x\ \Delta p_x = 2\pi\hbar$.By using de Broglie relation ($p=\hbar k$), the phase volume is given as

$$\Delta x\,\Delta y\,\Delta z \cdot \Delta k_x \Delta k_y\,\Delta k_z = (2\pi)^3 \qquad (2.2)$$

The density of states per unit energy per unit volume, which is shown by $\rho_{DOS}(E)$ give us a chance to find the total number of states per unit volume in an energy band with E_1 (lower) and E_2 (higher) according to

$$N = \int_{E_1}^{E_2} \rho_{\mathrm{DOS}}(\mathrm{E})\mathrm{dE} \tag{2.3}$$

It should be noted that N is the total number of states per unit volume, and $\rho_{DOS}(E)$ is the density of states per unit energy per unit volume. To find the density of states per unit energy dE, how much unit of k is taken place in the energy interval E and E+dE, as we already know that one unit volume of k-space carries two electrons of opposite spin.

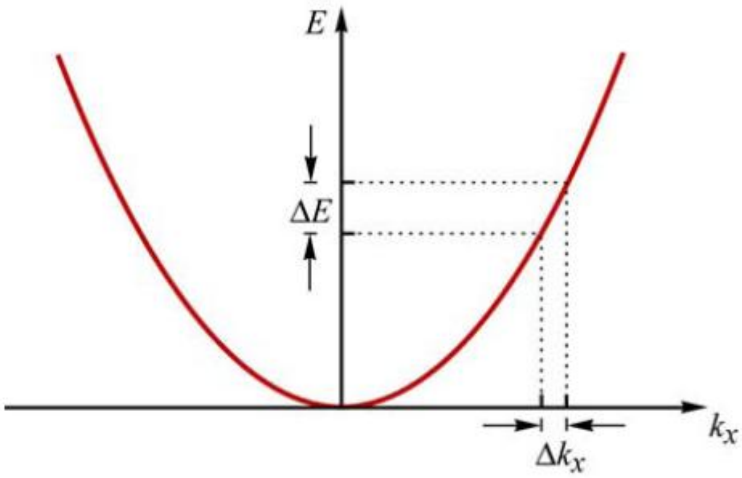

Figure 2.3 Parabolic dispersion relation with a k-space interval Δk and corresponding energy $\Delta E = (\partial E / \partial k_x)\Delta \mathrm{k}_x$

In order to find the volume of k-space between two energies, the dispersion relation should be applied. A one-dimensional, parabolic dispersion relation E=E(k_x) is shown in figure 2.3. The slope of the dispersion relation gives the k-space length associated with the energy interval.

To conceive of the features of semiconductors, the number density of electrons and holes in their respective bands are required. The result of the density of states available for occupancy in a particular band, and the probability that a state is engaged is adequate to that density [29]. In a study [30] it is given that is called as the law of mass action , for a non-degenerate semiconductor , which shows the product of electron density in the conduction band and hole density in the valence band for a given semiconductor for a given temperature does not change ($n.p=n_i^2$), frivolous of whether it is an intrinsic ($n=p=n_i$) or an extrinsic (n$\neq$p) semiconductor. Hence , if the density of electrons in the conduction band is raised by doping the semiconductor with donor impurities , the density of holes in the valence band will be reduced. For the non-degenerate situation, the total electron concentration in the conduction band is determined by following 2.4 expression

$$n = \int_{E_g}^{\infty} g_C(E) f(E) dE = \frac{1}{2\pi^2}\left[\frac{2m_C}{\hbar^2}\right]^{3/2} \int_{E_g}^{\infty} \frac{(E - E_g)^{3/2} dE}{1 + \exp[(E - E_g)/kT]} \quad (2.4)$$

where $g_C(E)$ is the number density of available states in the conduction band, $f(E)$ the Fermi-Dirac distribution function, the probability that the electron has an energy, E, m_c and m_v the effective masses of the electrons in the conduction band and holes in the valence band, severally. Similarly, the total hole concentration in the valence band for the non-degenerate limit is then formulized by

$$p = \int_{-\infty}^{0} g_V(E)[1 - f(E)] dE = \frac{1}{2\pi^2}\left[\frac{2m_v}{\hbar^2}\right]^{3/2} \int_{-\infty}^{0} (-E)^{1/2} \exp\left(\frac{E - E_g}{kT}\right) \quad (2.5)$$

Consequently , the expressions 2.4 and 2.5 could be rewritten for electron concentration in the conduction band and hole concentration in the valence band for the reference of zero energy taken at the top of the valence band;

$$n = N_C \exp\left[\frac{(E_F - E_g)}{kT}\right] \quad (2.6)$$

$$p = N_V \exp\left(-\frac{E_F}{kT}\right) \quad (2.7)$$

where N_C and N_V are the effective density of states in the conduction and valence band, respectively.

2.2.3 Optical Features in Semiconductors

To describe the interaction of light with electrons, there is a need to describe electron states. For this, Schrödinger equation describes behavior of matter in terms of wave function ψ [31].

$$\left[-\frac{\hbar^2}{2m}\frac{\partial^2}{\partial x^2}+V(x)\right]\Psi(x,t)=i\hbar\frac{\partial}{\partial t}\Psi(x,t) \qquad (2.8)$$

It is noted that “high curvature” corresponds to high energy for light waves and that the time dependence scales with the energy of the wave function. In free space and without potential, the solution of the Schrödinger equation for wave function will be in the form of

$$\psi_k(r) = Ae^{i\vec{k}\cdot\vec{r}} \qquad (2.9)$$

where the probability of finding matter at position r scales with $|\Psi|^2$ or $\Psi\times\Psi^*$

In a solid, electrons propagate in periodic potential; V(r) = V(r + a), defined by Bloch wave which is functional form of solutions to Schrödinger equation.

$$\psi_k(r) = u_k(r)e^{i\vec{k}\cdot\vec{r}} \qquad (2.10)$$

In other words, the function in equation (2.10) says implicitly that single atoms are surrounded by electrons; however, in a solid, electrons in neighboring atoms can interact. This modifies electron levels and results in energy bands.

2.3 SEMICONDUCTOR NANOSTRUCTURES

Low dimensional structures come into existence as one of fast growing technologies [32]. The size and the shape controllable semiconductors behave completely different from the original bulk ones. Quantum confinement (size) effects begin showing its acts on the structures less than ten nanometers in dimension. The motion of the current charge carriers in these nanostructures is limited in more than one dimension. The widening of the band gap is one of the familiar effects caused by quantum confinements, results from carriers coming into the possession of significant quantum energy of localization. With the help of effective mass theory, simple particle in-a-box estimations to define this behavior may act with a quite accuracy over a limited size regime. How such estimations can predict that the band gap of Si will have a growth due to one to three dimensional confinements over the one-to five nanometer size regimes is shown in figure 2.4.

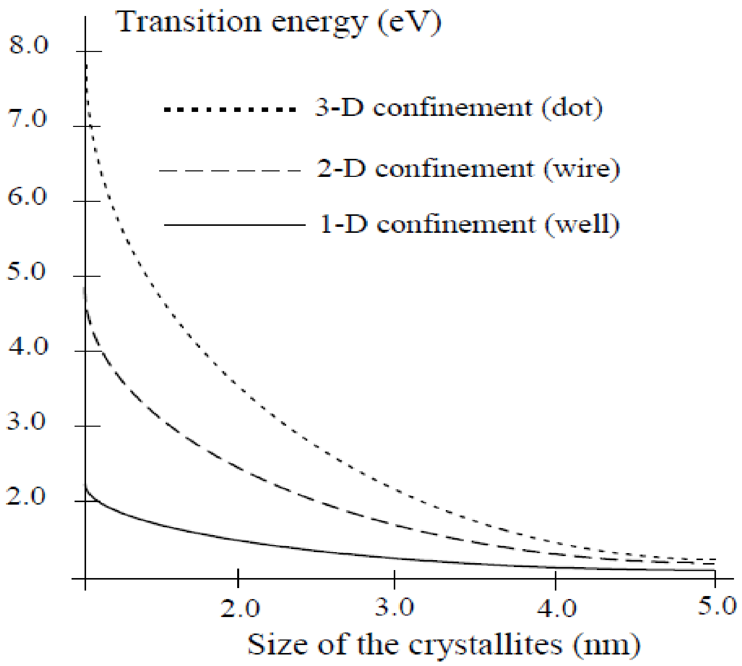

Figure 2.4 Si low-dimensional structures. Predicted band gap increase due to one-, two- and three-dimensional confinement in the *1-5 nm* regime [33]

There is clearly a need of need very small structures to alter the Si band structure dramatically, however, for both 2D confined quantum wires and 3D confined quantum dots the crystalline silicon band gap can change more than three times over this size domain. This reminds that the entire visible spectral range (*1.6-3.2 eV*) would be gotten as a function of particle size and shape.There are a few advanced epitaxial growth and lithography technologies for the formation of regular arrays of quantum wires and dots on semiconducting substrates. The average size of luminescent wire and dot arrays, however, is about 100-1000 nm with current lithography process. On the other hand, it can be generated much smaller nanostructures by a simple anodization process. Thus, it shows a way how to produce nanoporous silicon with pores less than 10 nm.

2.3.1 Porous Structures Creation

There is still a need to understand the whole mechanism of the anodic dissolution of silicon in fluoride media [33]. It's neglected in proposals for the mechanisms since about thirty years that the surface includes hydrogen molecules. There are recently some studies caring the reaction scheme as Lehmann and Gösele [34] gave. Gerischer *et.al.* [35] said another scheme about the reaction. A SiH_2 surface step site is initial thing for both mechanisms. Three different steps such as hole capture, electron injection and chemical steps are like in both mechanisms.

The porous silicon has high resistivity. The study shows that while quantum confinement effect causes an increase of donor binding energy, small size of the porous Si wires and Fermi-level pinning results in depletion at the surface. During porous Si formation the impedance measurements, the existence of surface state was established [36, 37].

The morphologies indeed have little differences, which involve two mechanism groups. The basic difference between two groups is that the main characteristic length in the first group is a screening length and in the second a diffusion length. The screening length appears more refined for porous silicon on p-type material where the process is insured by majority carriers. Whereas the diffusion length may be more relevant in the case of porous silicon on n-type material where the process is insured by light induced photo-carriers. The etching of n-type Si is more complicated. It has to be questioned that what would fix the scale of the smallest structures obtained in porous silicon.

Quantum confinement effects (QCE) is effective at the growing interface because tiny-scale [34] structures subsists in porous silicon and ruling the porous silicon morphology, the tiniest-scale structures getting frozen caused by carrier depletion. This effect should show compatibility to illumination. For instance as a consequence of QCE, a very slim line PS wire will have electron states the bulk silicon gap, lower than only above an effective bandgap. In a wire like this, if the energy of the photon is larger than this effective band gap photo-carriers will be occupied, so as higher energy illumination is a needed to form small-scale structures.

In reports of Lehmann and Gösele [38], the experimental evidence of this ideas could be found.

Due to the macropores in some place whose characteristic size and spacing appear ruled by the screening length in the substrate material it contains, the morphology of n-type of porous silicon substrates is not very similar to that of a p-type [39, 40, 41]. In the case of p-type silicon substrates the space charge acts as a block for holes, and the field is large enough to open the gaps at the top of the barrier around pore tips, while, the n-type behaves as a sink, channeling the holes to the pore tips. This different energetic configuration may have a relationship with an unlike morphology. Additionally, there is evidence in n-type PS that construction of the macropores might be considered as the favorite in the nearby region of ionized donors [42]. Nanostructures are also found along with macropores, in particular under the applied front-side illumination [43]. The basis of these nanostructures might have characteristics related to that in p-type Si substrates. It can be considered that these are the fundamentals for the formation of PS and the quantitative improvement of the models above gives a full understanding of the mechanisms.

2.3.2 PL in Nanocrystallites (PS)

After the discovery of strong visible photoluminescence from electrochemically-etched silicon by L. Canham, a numerous studies on silicon nanostructures have been published [44]. Still, the PL base is not yet steadfastly grasped. Quantum confinement in silicon nanocrystallites is the most taken explanation [45, 46], on the other hand, localizing states at the surface of the crystallites, e.g. due to dangling bonds, might also make an important contribution [47, 48]. Different calculations of the energy gap as a function of the size of crystallites have been recapitulated and argued the predicted radiative recombination times and significance of phonon-assisted transitions by Delerue *et.al.*[49]. Surface dangling bonds and acceptor (or donor) impurities were thought for realizing the mechanisms of visible luminescence from the nanocrystallites semiconductors.

2.3.3 Energy-Size Correlation

It is given by Delerue *et.al.* [49] that an empirical linear combination of atomic orbitals (LCAO) method including the interatomic terms migth possess an application to the calculation of the electronic states of silicon nanoclusters (~*4nm*). The zero dimensional case is tantamount to the highest confinement energy in the model. The energy range for the major experimental luminescence of porous silicon changes from 1.4 eV to 2.2 eV. This is logical to crystallite sizes between *2.5* and *4.5 nm* [50]. An important thing is that a dependence of $d_{-1.39}$ for the energy gap as a function of the crystallite diameter, *d* was estimated by some methods. This is dissimilar with a big amount from the d_{-2} law which would be gotten from effective mass theory [51].

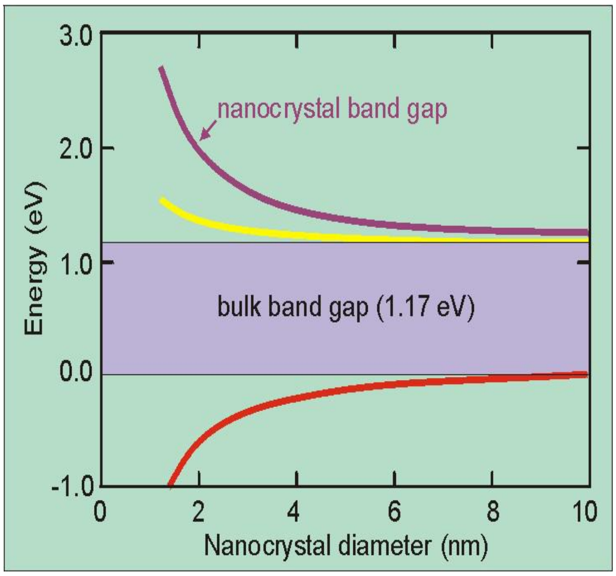

Figure 2.5 Energy versus nanocrystal diameter [52]

2.4 OPTICAL FEATURES OF SILICON NANOSTRUCTURES

Several authors [53, 54, 55] studied on some articles states the optical features of porous silicon created by electrochemical dissolution. there is an inverse due to the quantum confinement of electron-hole pairs in Si nanocrystallites relationship between the optical gap energy and the average nano-particle size (see Figure 2.5) from the measurements of the optical absorption spectra.

2.4.1 Photoluminescence:

There are extremely sharp characteristics lines which are found in the absorption and emission spectra of nearly isolated atoms and ions due to transitions between quantum levels. This causes their wavelengths or photon energies can be calculated with a great accuracy. The lines are like fingerprints for a particular atom or ion. Hence, it may be used for identification processes. Molecular spectra are also sharp while it is generally less sharp than atomic spectra. To verify the electronic structure of molecules, the point of spectral lines in terms of position can be carried out with a very good accuracy. In solids, the interactions cause the large degeneracy of the atomic levels split into quasi-continuous bands (valance and conduction bands) and makes their optical spectra rather broad.Fundamental gap is a product of the energy difference between the highest lying valences (the highest occupied molecular orbital, HOMO) and the lowest lying conduction (the lowest unoccupied molecular orbital, LUMO) bands. In visible light region, penetration depths of electromagnetic radiation are on the order of 50 nm. Applications of absorption spectroscopy for the characterization of bulk solids is limited by such a small penetration depth, however it is still applicable for the characterization of nanostructures and nanomaterials [56] . In figure 2.6 shows that decreasing diameters of nanocrystals reveals increasing band gap.

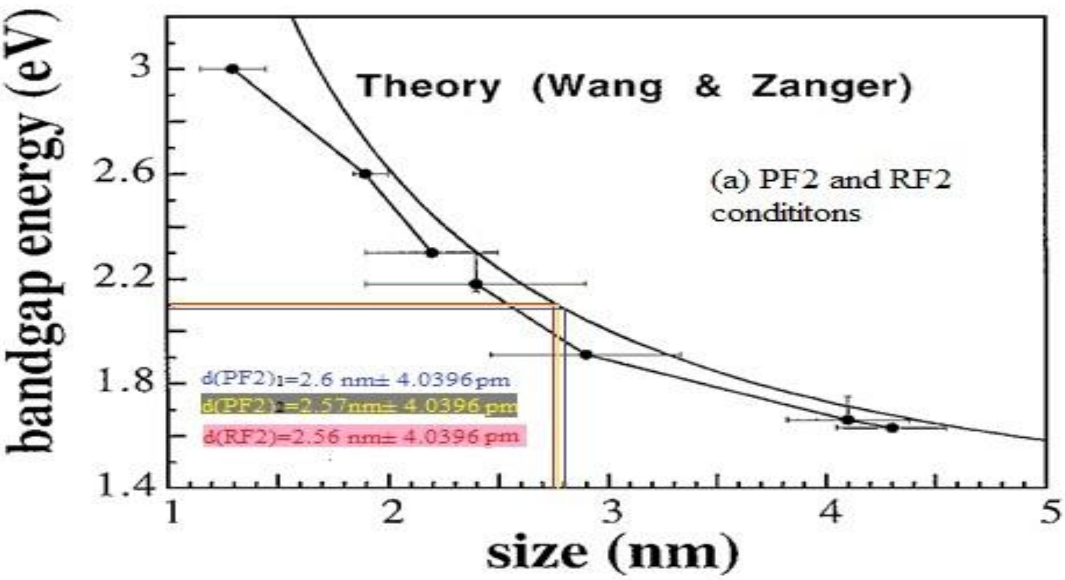

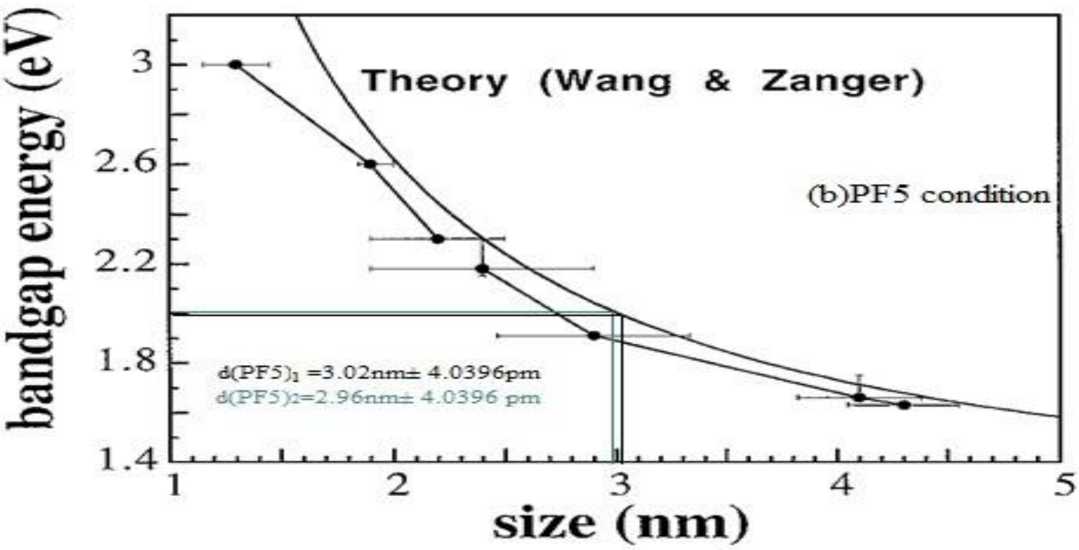

Figure 2.6 One electron band gap calculated in [57] (continuous line) and experimental band gap measured in [58,59] circles versus crystallite size: blue and yellow color lines drawn for PF2 condition, and red color line for RF2 conditions, (b) Dark gray and green lines are given for PF5 condition.

Luminescence means that the emission of light by a material through any process other than blackbody radiation [60]. The emission of light can be because of a variety of stimulations. For instance, when the emission is due to electronic stimulation, it is called as Cathodoluminescence (CL). One more example can be given as X-ray fluorescence, when high-energy photons, i.e. X-rays, are used to excite the sample. In PL, one measures physical and chemical properties of materials and analyzes how the relaxation of optical emission occurs after photons induce excited electronic states in the material system. In this process, ligth is generally directed onto the sample for excitation, and the emitted luminescence is collected by a lens and passed through an optical spectrometer onto a photon detector. Electronic transition probabilities within the sample are related to the spectral distribution and time dependence and time dependence of the emission which can be used to give qualitative and, sometimes, quantitative information about chemical composition, structure, impurities, kinetic process and energy transfer. Sensitivity is one important result of PL technique, allowing very small quantities (nanograms) or low concentrations (parts-per-trillion) of material to be analyzed. Without controlling the conditions carefully, precise quantitative concentration determinations are difficult, and many applications of PL are primarily qualitative. In PL, a material gets energy by absorbing photon at some wavelength by causing an electron promoted from low to higher energy level. This may be defined as making a transition from ground state to an excited state of an atom or molecule, or from valance band to conduction band of a semiconductor crystal or polymer (electron-hole pair creation). Via interactions with crystalline or molecular vibrational and rotational modes, system then makes a non-radiative internal relaxation, and the excited electron moves to more stable excited level, like bottom of conduction band or lowest vibrational molecular state. Electron will return to the ground state after a characteristic lifetime in the excited state. In luminescent materials, some or all of the energy is released in the form of light during this final transition, where the relaxation is known as radiative. The wavelength of the emitted ligth is longer than that of the incident light. I should also be known that fast PL with a life of submicrosecond is called as "fluorescence", on the other hand slow ones 10^{-4} to 10 s, are called "phosphorescence." Optical absorption and photoluminescence spectra are usually used in the obtaining information about the size of nanocrystals of semiconductors [61,62]. Figure 2.6 clearly represents the energy or wavelength part of PL spectra has relation with band gap of Si nanocrystallites and obviously shows band gap of nanocrystallites increases with a decreasing size. [61]

2.4.2 Quantum Confinement Effect

Quantum size effect plays an important role for formation of unique optical property of nanomaterials. When the de Broglie wavelength is greater than the size of nanocrystallite (i.e. single crystal nanoparticle), electron and holes are limited to move in some directions and known as confined and electric dipoles are created, and discrete electronic energy level would be formed in all materials. Separation between adjacent levels increases with decreasing dimensions.

Figure in 2.7 shown below schematically represents such discrete electronic configurations in nanocrystals, nanowires and thin films; similar to a particle in a box, the energy separation between adjacent levels increases with decreasing dimensions. Figure 2.7 schematically illustrates such discrete electronic configurations in nanocrystals, nanowires and thin films; the electronic configurations of nanomaterials are significantly different from that of their bulk counterpart [56].

Systematic changes in the density of electronic energy levels as a function of the size causes these transformations and these alterations cause to strong variations in the optical and electrical properties with size [63,64]. Nanocrystals take place in between the atomic and molecular limit of discrete density of electronic states and the extended crystalline limit of continuous band [65].In any material, there will be a size below which there is a substantial variation of fundamental optical and electrical properties with changing size when energy level spacing exceeds the temperature. For a given temperature, this happens at a very large size (in nanometers) in semiconductors as compared to metals and insulators. In metals, where the Fermi level takes place in the center of a band and the relevant energy level spacing is very small, the electronic and optical properties more closely looks like those of continuum, even in relatively small sizes (tens or hundreds of atoms) [66,67]. In semiconductors, the Fermi level take place in between two bands, so that the edges of the bands are dominating the low-energy optical and electrical behavior.

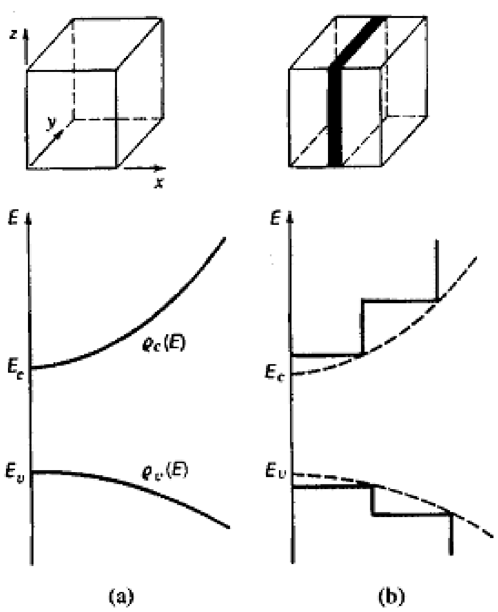

Figure 2.7 Schematic illustrating discrete electronic configurations in nanocrystals, nanowires and thin films and enlarged band gap between valence and conduction bands.

Optical excitations across the gap are dependent strongly on the size, even for crystallites as large as 10,000 atoms. The energy band gap is already large enough in the bulk form for insulators .The quantum size effect is most familiar title for semiconductor nanoparticles, where the band gap increases with a decreasing size, causing in the interband transition shifting to higher frequencies [68-71]. The energy separation in a semiconductor, i.e. the energy difference between the completely filled valence band and the empty conduction band is of the order of a few electron volts and increases rapidly with a decreasing size [70] .

2.4.3 Chemistry of PS

Even though there is still debate about origin of PL, quantum size effect is thought as one of the major sources for the red PL [72]. As shown in 1990, a judgment on the origin of PL in PS in the light of mass of evidence reasonable by according to the recent review by Calcott in 1998. He made five alternative models which sums up of quantum confinement model [73 (a)]. However, the more efficient one is claimed to be the quantum size effect [73(b)]. On the other hand, the PL peak wavelength and the intensity are associated with dependency on the surface chemistry of the PS, particularly by trusting the relative amounts of O and H on the surface [74, 75]. It is found that the PL quantum efficiency, wavelength dependence, and lifetime are sensitive to oxidation of the PS and to the surface adsorbates (solvents) [76]. The results of the studies presented that surface passivation by either H [77] or O [78] to have dangling Si bonds creates intense PL. In addition, the oxidized PS at high temperature gives out a stable red PL, whilst in the condition of freshly- prepared hydrogenated samples the PL intensity is sensitive to the external environment [79].

2.4.4 Blue PL and Oxidation Effect on PL peak

It is thought that oxidation of PS surface was showed to create blue PL [80]. Just after formation of PS, blue PL is weakly found, but it turns into intense only after strong oxidation [81]. Excitation intensity and emission wavelength does not alter the (blue) PL decay. With a decay time around 1ns, it has a non-exponential form [82]. The blue PL which occurs faster than the red PL, necessitates surface oxidized PS. The discussion for origins of this is still went on. Some models suggested as band to-band recombination in Si nano-crystals, emission from oxides, and emission due to surface states are considered [83]. The indications can be expressed by the blue PL may arise from the small c-Si core region which cannot be guessed as surface state emission, while the red PL possibly proceeds from the near-surface region of the Si crystallites [84,85].

2.4.5 Relationship between Band gap energy and Optical absorption

It is known that by reducing the size of nano-crystallite or incrising porosity, the optical absorption edge shifts to higher energy [86]. Nevertheless , a weak absorption tail is getting visible to lower energy. Suda *et.al* [87] gives the result that a surface optical gap that evidently has a correlation with the red PL energy, presenting that the surface atomic configuration has relation with the PL origin. The change in the PS optical gap proportional to that of bulk crystalline Si is found to be nearly have to the same total quantity of the shifts in the conduction and valence band edges, which further affirm the quantum confinement mechanism.

2.4.6 Porosity effects on PL spectra

The PL spectra acquired at different temperatures on different porosity samples shown by Di Francia *et.al*. [88]. It is given that a blue-shift the PL peak of the high porosity (80%) samples and 10 K on diminishing the temperature, whilst, in the case of medium porosity (60%) samples, the peak place of the PL spectra at the same temperature chain is only slightly affected. Moreover, the spectrum of high porosity samples with respect to that of medium (160 meV) ones, taken at 10 K, is characterized by a much larger FWHM (360meV). These entire features have been explicated by assuming the PL emission for each sample that comes from a different dispersion of limited quantum structures [89]

CHAPTER 3

3. FABRICATION TECHNIQUE

3. 1 SILICON WAFER CLEANING BEFORE ETCHING PROCESS

Surfaces could be described by scientists as hydrophobic or hydrophilic. SiO_2 surfaces are instances of hydrophilic ones. Hydrophilic surfaces could get wet easily by cleaning solutions. Any particles on the hydrophilic surfaces have a tendency to be in solution till the solution is removed from the surface during drying process. Si surfaces without oxide are hydrophobic. We cannot clean hydrophobic surfaces and cleaning solutions do not make them wet easily. Solutions tend to “bead” up on the surface during drying process and leave particles on the surface rather than keeping them in solution.

In figure 3.1 an analytical method which defines whether a surface is hydrophobic or hydrophilic is shown. Contact angle can be measured by this method.

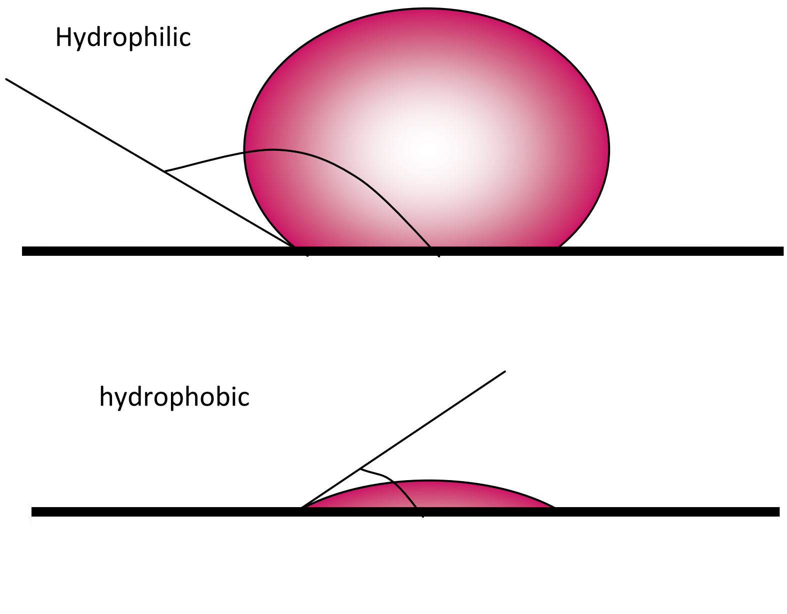

Figure 3.1 Wetting Behavior and contact angle

The standard RCA method studied by Werner Kern and he published a paper called "first systematically developed wafer cleaning process for bare and oxidized Si" in 1970 [90, 91]. The clean that Kern made known had been in use at RCA since 1965 [91] and went on to become known as the "RCA clean" - the most widely used clean in the industry.

The RCA clean is known as a FEOL clean. The original RCA clean sequence is [91]:

•Standard Clean 1 (SC1) - 5 volumes of H_2O, 1 volume hydrogen peroxide (H_2O_2) 30%, 1 volume ammonium hydroxide (NH_4OH) 29% at 70 - 80^{o}C.

•Ultrapure water rinse.

•Standard Clean 2 (SC2) - 6 volumes H_2O, 1 volume H_2O_2 30%, 1 volume hydrochloric acid (HCl) 37% at 70^{o}C.

•Ultrapure water rinse and dry.

The SC1 clean takes out organic residues and particles. The SC1 clean works by creating and dissolving hydrous oxide films. The SC2 clean takes alkali metal and hydroxides - Li, Al, Ti, Zn, Cr, Fe, Ag, Pd, Au, S, Cu, Ni, Co, Pd, Mg, Nb, Te, W, Na, Fe (leaves Cl residues) out.

The execution of the RCA clean is crucial. So as to provide H_2O_2 it is commonly used stabilizers such as sodium phosphate, sodium stannate and with containing high levels of aluminum. The important point is that it must be used high purity semiconductor grade chemicals with un-stabilized H_2O_2 to prevent recontamination of wafers. And also H_2O_2 has a confined bath life and decomposes over time. So as to assure proper cleaning activity solution change-outs must be devised. Deficient H_2O_2 levels in SC1 baths can have a conduction to surface pitting and insufficient H_2O_2 levels in SPM baths lead to carbon build-up in the bath and poor stripping of organics.

In the industry areas various forms of the RCA clean have been used. Prior to 1997 a "typical" execution could be:

•Sulfuric Peroxide (SPM) - 4 volumes of sulfuric acid (H_2SO_4) 98%, 1 volume H_2O_2 30% at 130^{o}C for 10 to 15 minutes.

•Ultrapure water rinse.

•Dilute hydrofluoric acid (DHF) 50 volumes H_2O, 1 volume hydrofluoric acid (HF) 49% at room temperature for 10 seconds.

•Ultrapure water rinse.

•SC1 for 20 minutes.

•Ultrapure water rinse.

•SC2 for 15 minutes.

•Ultrapure water rinse and dry.

The SPM makes the bulk organic removal and chemically oxidizes the wafer surface in the anteceding sequence, the DHF removes the chemical oxide, SC1 removes particles and SC2 removes metals.

Thin chemical oxide layer left on the wafer surface by the RCA clean could not be endured if RCA clean is executed prior to metallization, epitaxial growth or thin gate-oxidation. Moreover, the succession is changed to the so-called HF last process where DHF is the last chemical step prior to rinse and dry. We must use special care in rinsing and drying due to the HF last process is used a hydrophobic surface results.

3.2 CHEMICAL STAIN ETCHING PROCESS

The most employed method for producing porous silicon is anodization method because of the fact that the rest methods like stain etching do not give enviable results in terms of homogeneity of produced porous silicon and repeatability of experiments. However, applied bias current causes the group processing impossible and stop compatibility with silicon technology [92]. This does not happen in stain etching process.

In stain etching, Hydrofluoric acid is used to etch silicon surface and Nitric acid (HNO_3) is oxidizing agent. In addition to the HF-HNO_3 solution, the effect of surfactants were searched with different concentrations and etching time. In the first part of the experimental part, the HF/HNO_3 ((400ml/1ml)) solution has been prepared for PS formation. After doing this process, the RF2, PF2 and PF5 surfactant with variable concentrations such as $83.2*10^{-3}$ ml, $83.2*10^{-3}$ ml, $208*10^{-3}$ ml respectively have been tried. In all processes, the produced PSs were dried with Argon gas and put into ambient air.

3.2.1 Mechanisms of Stain Etching Process

The general reaction involving the dissolution of silicon oxide in HF solution can be expressed as

$$HNO_3 + 3H^+ = NO + 2H_2O + 3h^+ \tag{3.1}$$

$$nh^+ + Si + 2H_2O = SiO_2 + 4H^+ + (4-n)e^- \tag{3.2}$$

$$SiO_2 + 6HF = H_2SiF_6 + 2H_2O \tag{3.3}$$

$$3Si + 4HNO_3 + 18HF = 3H_2SiF_6 + 4NO + 8H_2O + (4-n)h^+ + (4-n)e^- \tag{3.4}$$

These are predicted reactions in stain etching process; however they are still the subject of discussion. For many reports on the kinetics of silicon oxide etching, determining the fluoride species in the solution responsible for the etching reactions has been on mind. This is because HF is a weak acid, which ionizes only partly to fluoride ions, and its aqueous solutions might contain much amount of fluorine in the form of un-ionized HF and partially ionized bifluoride HF_2^-. A number of ways may be possible in the formation of surface species leading to breaking of the Si–O bonds as has been suggested [93] figure 3.2 shown below:

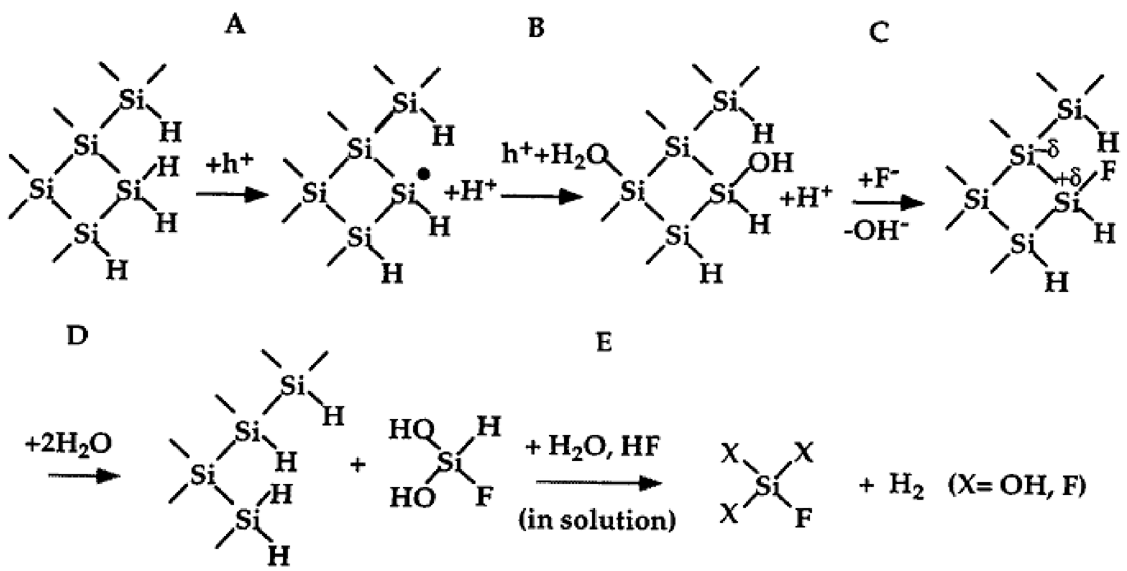

Figure 3.2 Possible reaction pathways resulting in the dissolution of a silicon atom in HF [93]

3.2.2 Structure and Effects on materials of Surfactants

Surfactants are compounds that decrease the surface tension of a liquid, making easier spreading, and lowering of the interfacial tension between two liquids, or between a liquid and a solid. In general, there are three types of surfactants: detergents, wetting agents and emulsifiers. The term surfactant is a blend of surface active agent. Surfactants are habitually organic compounds that are amphiphilic, meaning they comprise both hydrophobic groups (their tails) and hydrophilic groups (their heads). Therefore, they are able to be dissolved in both organic solvents and water.

Surfactants lower the surface tension of water by adsorbing at the liquid-gas interface. They also decrease the interfacial tension between oil and water by adsorbing at the liquid-liquid interface. Many surfactants can also gather together in the bulk solution into aggregates. Vesicles and micelles are examples of such aggregates. The concentration at which surfactants start to create micelles is known as the critical micelle concentration (CMC). When micelles form in water, their tails form a core that can encapsulate an oil droplet, and their (ionic/polar) heads form an outer shell that maintains favorable contact with water. When surfactants assemble in oil, the aggregate is referred to as a reverse micelle. In a reverse micelle, the heads are in the core and the tails maintain favorable contact with oil.

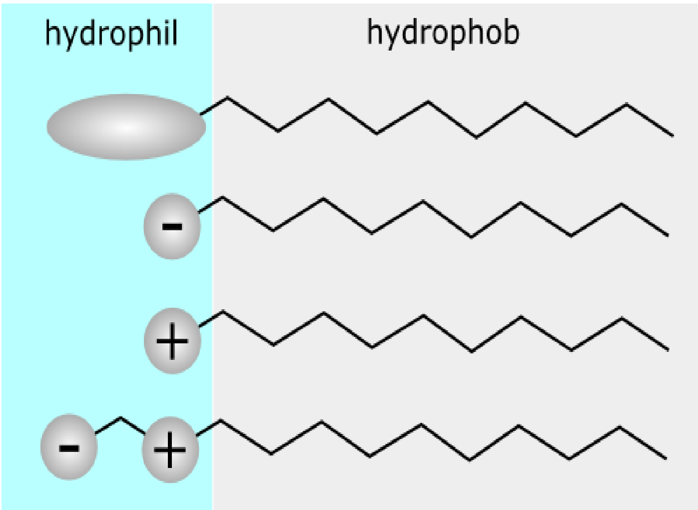

Figure 3.3 Surfactant classification according to the composition of their head: nonionic, anionic, cationic, amphoteric

A surfactant can be classified by the existence of formally charged groups in its head. There are no charge groups in its head if it is a non-ionic surfactant. The head of an ionic surfactant has a net charge. If the charge is negative, the surfactant is more specifically known as anionic; if the charge is positive, it is known as cationic. If a surfactant comprises a head with two oppositely charged groups, it is termed zwitterionic (dual charge) as it is given in the figure 3.3 [94].

CHAPTER 4

4. CHARACTERIZATION TECHNIQUES

4.1Photoluminescence (PL) and Photoluminescence Excitation (PLE) Spectrometry

Luminescence is known as the emission of absorbed light by a substance exposing with electromagnetic radiation of sufficiently short wavelength. It happens when an electron returns to the electronic ground state from an excited state and loses its excess energy as a photon. Singlet states and triplet states is the electronic states found in most organic molecules. A molecule in the single state start emitting photons when exposed to electromagnetic radiation and cease emitting when the source is off. On the other hand, a molecule in the triplet state, it decays step by step emitting photons of lower intensity each time it decays. The phenomenon is known as photoluminescence and the study of emitted light is photoluminescence spectroscopy.

This results each material has its certain emission and absorption wavelength like fingerprints. Another technique, photoluminescence excitation (PLE) spectroscopy, for revealing the excitation wavelength of the substance is used so that photoluminescent process occurs [95].

So as to find PL/PLE peaks of a photoluminescent material like porous Si, a PL/PLE system was used for this aim given in figure 4.1 below. A white light (wavelength=1 nm) is sent into monochromator 1 is shown in picture below as Mono 1. This will supply us to choose a tunable range for incident beam such as 350 nm wavelength of UV light. After this process, UV light is focused on porous sample that has an emission in visible region around 620 nm wavelengths. Hence, it’s an evidence to be porous for the samples which has visible photoluminescence property. In this aspect for PL measurements, monochromator 2 is adjusted to be selecting the range of visible outgoing light between 580 nm and 680 nm so that the Photomultiplier tube will detect in the defined range.

On the other hand, for the PLE measurements, Monochromator 1 is important in order to find the excitation wavelength which is defined and emitted from the source to the sample in order to have the best PL characteristics.

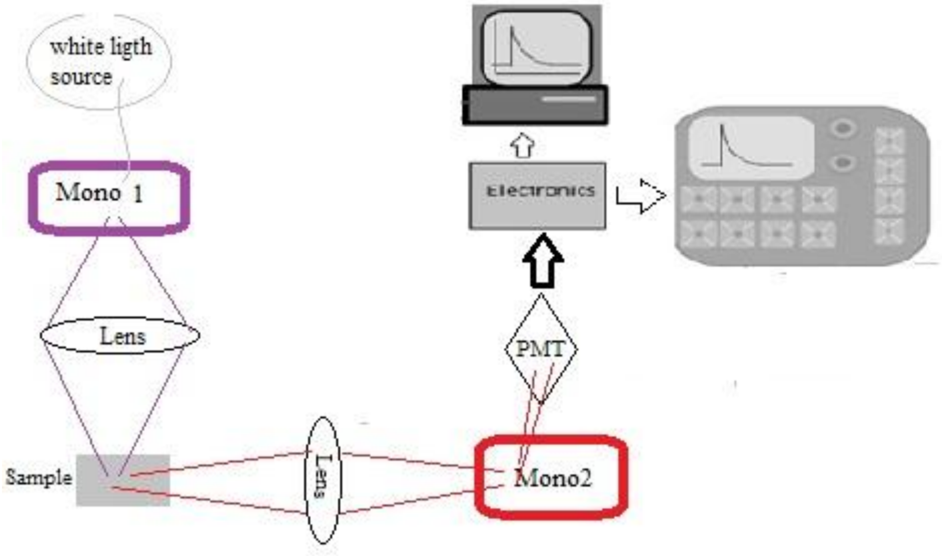

Figure 4.1 Scheme of PL/PLE systems

4.2 X-Ray Photoelectron Spectrometry (XPS)

The basic and methodologies of X-ray Photoelectron Spectroscopy (XPS) is taken place in this section and it is briefly discussed. The unique energy levels of the emission of photons (X-ray) or electrons ejected from the atoms define electronic spectrum of specimen [96]. As it is illustrated in Figure 4.2 when an incident electron or photon, such as X-ray, have an interaction with an unexcited atom, an electron from an inner shell is sent out and is left a hole or electron vacancy in the inner shell in figure 4.2b. By lowering its energy an electron from an outer shell fills the hole, and simultaneously the excess energy is sent through either emission of an X-ray in figure 4.2c ejection of a third electron that is known as an Auger electron in figure 4.2d from a further outer shell. Both X-ray and Auger spectral lines are characteristic of the element like fingerprints because each atom in the Periodic Table has its own electronic structure with a unique set of energy levels. The chemical compositions of a material can be found due to measuring the energies of the X-rays and Auger electrons emitted by a material.

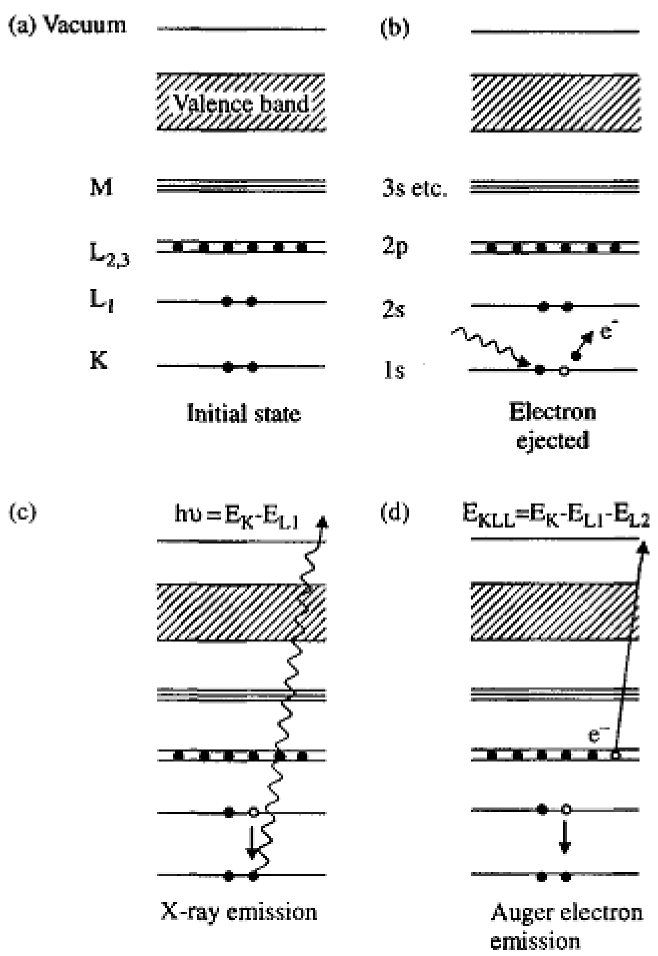

Figure 4.2 Schematic of electron energy transitions: (a) initial state, b) incident photon or electron ejects K shell electron, (c) X-ray emission when 2s electron fills electron hole, and (d) Auger electron emission with a KLL transition [96].

The binding energy (*BE*) of photoelectrons is written down the difference in excitation energy (ε) of X-ray source and kinetic energy (*KE*) of photo-electron.

$$BE = \varepsilon - KE \tag{4.2}$$

Since values of the binding energy are element-specific, atomic identification is possible through measurement of photoelectron energies [56].

4.3 Confocal Microscope (CSLM)

A conceptual understanding of how a confocal scanning laser optical microscopy (CSLM) is a necessecity for luminescent studies. Indeed, confocal microscopy bases on the luminescence which is emission of photons of lower wavelength generated by hitting sample atoms by an incoming wave. In other words, absorbtion of an incident wave will be released with a different color. To see the difference between confocal and widefield microscope, let us look what is the working principle of these two microscopes. In a tradional widefield microscope, all sample is illuminated simultaneously, however, in confocal microscope,

a beam laser ligth is scanned in the small part of the sample. This occurs by formation point by point image[97]. The basic components of confocal microscope is given below in figure 4.3.

The most important part for the resolution of the image taken from confocal microscope is pinhole which blocks incoming light from out of focus. Hence, rejecting of out-of-plane unfocused light let us obtain a sharper, better resolved image. The optimum resolution is obtained by a tunable pinhole. On the other hand, dichroic mirror is used to reflect light shorter than a particular wavelength but transmits light of longer wavelength. Thus, the light from the main source is reflected and sent through the objective to the sample, while the longer-wavelength light from the fluorescing specimen is sent through both the objective and the dichroic mirror. Furthermore, it is possible to construct 3 D shape of a volume of the specimen by collecting the data of a series of thin slices taken along vertical axis, it is z axis in this study [98]. For this, the detector is connected to a computer which forms the image one pixel at a time. For instance, a 512pixel x 512 pixel image is typically achieved at a frame rate of 0.1 to 30 Hz. In a study [99] , the main two advantage of confocal microscope is written down below as:

- Instead of at different angles as in the case of the scanning mirror configuration the specimen is everywhere exposed with ligth axially, therefore avoiding optical aberrations. Thus, the uniform illumination of the entire field of view is possible.
- by handling the amplitude of the stage movements like increasing, the field of view can be augmented more than that of the static objective.

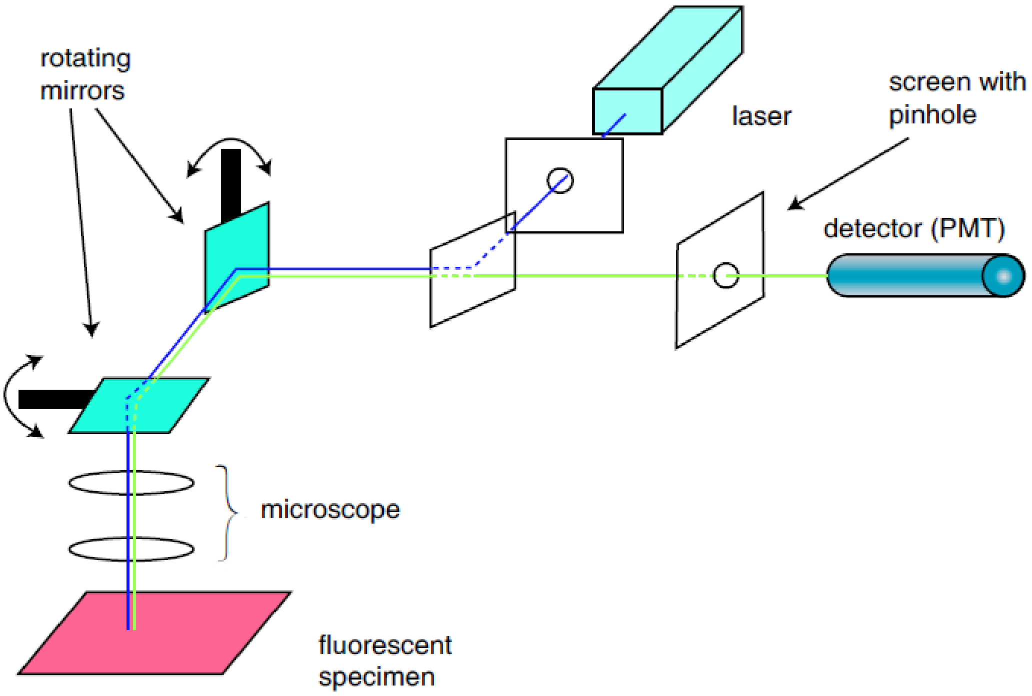

Figure 4.3 Basic components of a confocal microscope. Light beam from the laser is scanned across the specimen by using the scanning mirrors. Optical sectioning happens as the light passes through a pinhole on its way to the detector [98].

CHAPTER 5

5. RESULT AND DISCUSSIONS

The formation and investigation of PS have been employed for acquiring information about how to create uniform photoluminescence from PS by using stain etching method under addition of two types of surfactant with various etching time. The etching time versus type of surfactant is given below in the table 5.1:

Table 5.1 The etching time versus type of surfactant

Time(minute)	Without Surfactant	RF2	PF2	PF5
t_1	2	2	2	2
t_2	5	5	5	5
t_3	7	7	7	7
t_4	10	10	10	10
t_5	12	12	12	12

5.1 Photoluminescence Excitation (PLE) Results

This technique measures the excitation wavelength which is needed to be able to agitate the valence electron of the porous Si from its ground state to corresponding excited state. In other word, this means, the electron will move from the valence band of porous Si to conduction band. This will provide to form electron-hole pairs. The results for PLE are represented below in figure 5.1 with respective to type and concentration of surfactant and without surfactant.

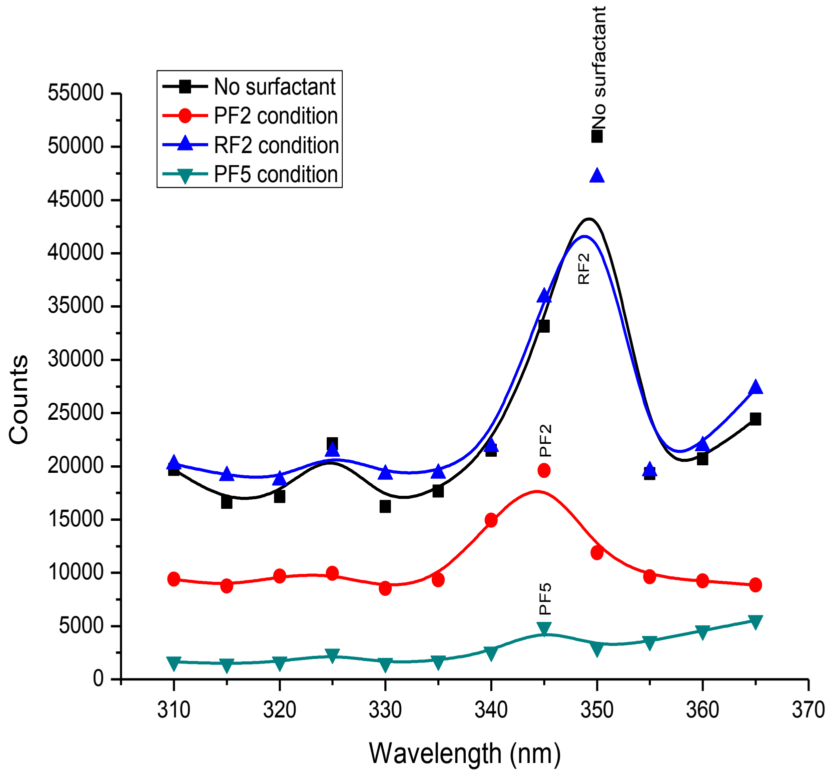

Figure 5.1 PLE Spectrum of PS under different concentration of various surfactants and without surfactant.

There is a variety of excitation wavelengths among PF2, PF5 as 345 nm and RF2, without surfactant as 350 nm. Excitation wavelength of PS formed under PF2 and PF5 conditions has almost the same pore size of PS pores. However, the excitation wavelength for PS formed under RF2 conditions is different from PF2 and PF5 conditions because of the difference in pore size distribution.

5.2 Photoluminescence (PL) Results

It is the base of this study in the view of structure and photoluminescence properties. Namely, if the semiconductor has a photoluminescent effect, it represents that the surface of the particular semiconductor, Si in this study, has nanopore layers on it. The PL spectra of porous Si studied under three different conditions such as RF2, PF2, and PF5 are took place in figure 5.2, in figure 5.3 and in figure 5.4 respectively.

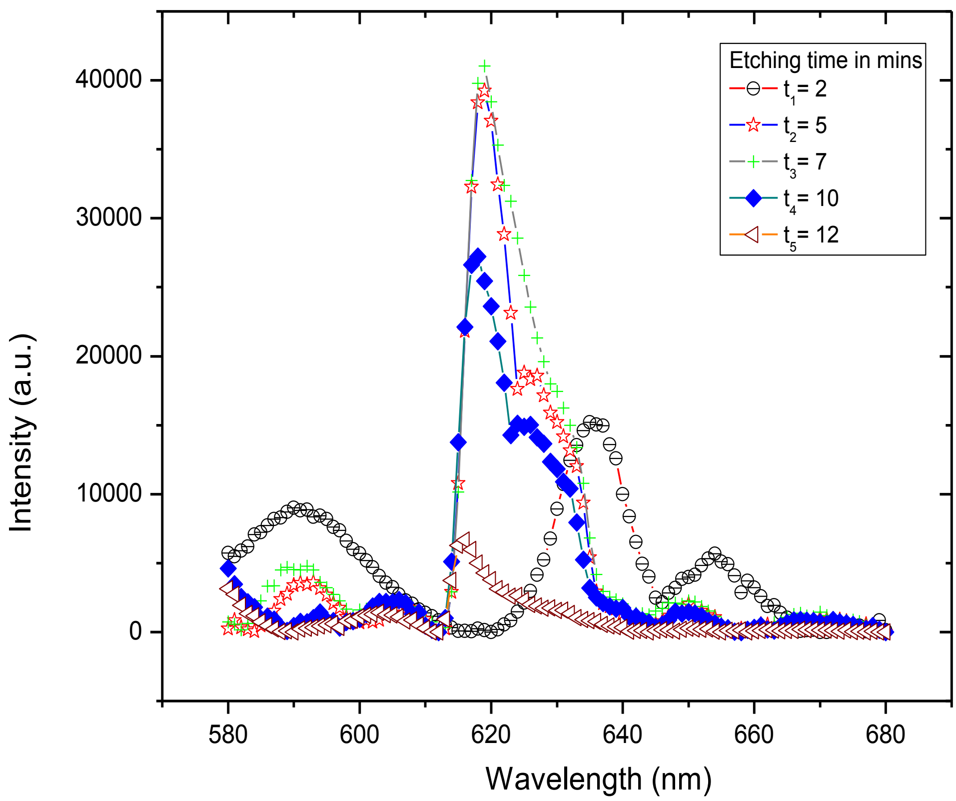

Figure 5.2 PL spectrum of Porous Si formed under RF2 condition with increasing etching time.

For RF2 condition, as it is seen in figure 5.2 above, the best PL peak obtained in this study has been shown with blue color which has an etching time of 7 minutes. The reason for this graph is related to formation process of pore structure. In the graph shown with black color, it shows that the initiation of porous surface was successful at the end of 2 minutes of etching time. From this point, we understand that etching time will contribute to the formation of pore structure until 7 minutes. Just after this point, the pore structure will be becoming a polish surface. Hence, the decrease in the height of nanopillars will cause decrease in the peak and at last, the reflection of the incoming ultraviolet light will occur. In addition, at the end of 2 minutes, the peak value begins changing from 640 nm through 620 nm by increasing etching time.

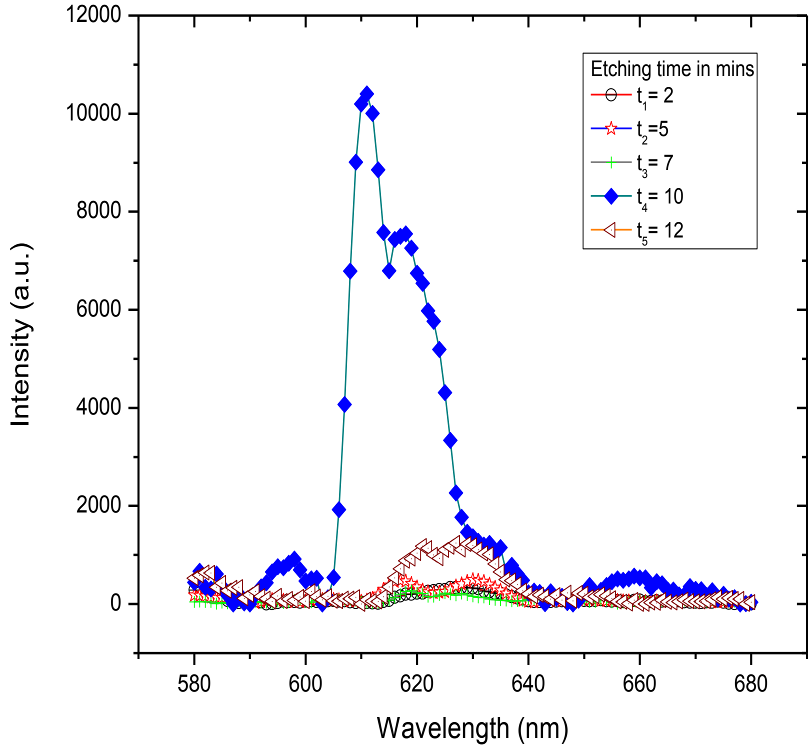

Figure 5.3 PL spectra of porous Si formed under PF2 condition with increasing etching time.

The figure 5.3 given for PF2 condition represents that there is a sharp increase in the peak of wavelength of porous silicon formed during the etching time of 10 minutes. Moreover, for the etching time of 10 minutes, there are two different peaks centered at 617 nm and 621 nm which stems from two different pore size distributions throughout the porous Si. On the other hand, it almost becomes polished quickly for the etching time of 12 minutes.

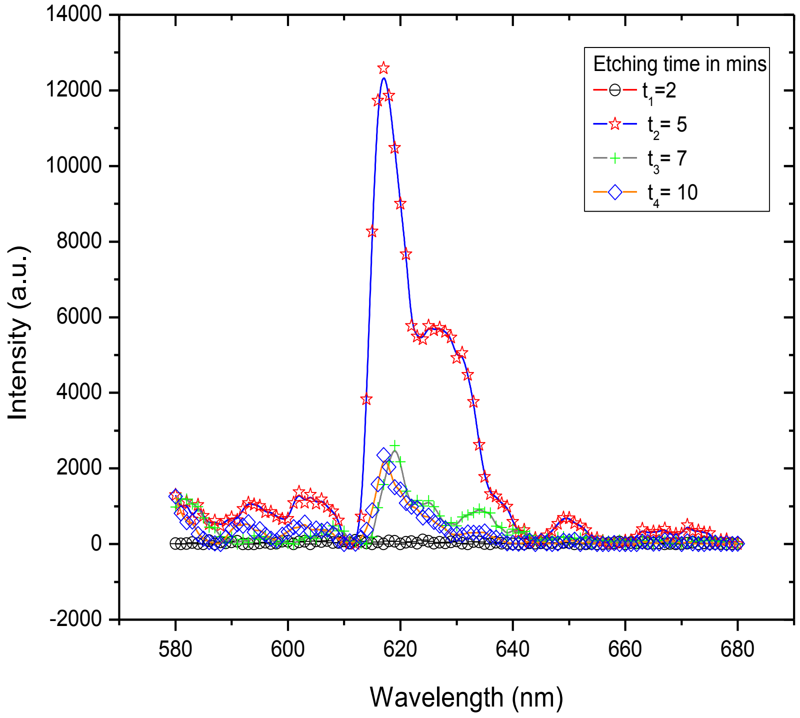

Figure 5.4 PL spectrum of Porous Si formed under PF5 condition with increasing etching time.

The figure 5.4 shown above for PF5 condition states that the optimum time for formation of porous Si is the etching time of 5 minutes. Like PF2 condition, there have been two peaks of wavelength centered at 616 nm and 627 nm. This is again the result of two different pore size distribution of the porous Si obtain for the etching time of 5 minutes

5.3 X-Ray Photo-electron Spectroscopy (XPS) Results

From X-Ray Photo-electron Spectroscopy, each energy or wavelength in the spectroscopy will match a specific atom type due to their certain binding energy. The binding energy is given by the difference in excitation energy of X-ray source and kinetic energy of photo-electron.

$$BE = \varepsilon - KE \tag{5.1}$$

Hence, the results of counts of photoelectrons versus binding energy of core electrons will be given for p-type Si crystal which is cleaned via RCA method, for porous Si formed at first without surfactant, and then under RF2, PF2, and PF5 conditions respectively. Bayliss at al. [100], Sham at al. [101], Francia at al.,[102] and others have dealt with X-ray absorption fine structure to determine surface bonding, while Bangert at al. [103] activated luminescence by using X-ray around the Si K edge. XPS studies [104-113] have focussed mainly on correlating surface composition and oxidation state.

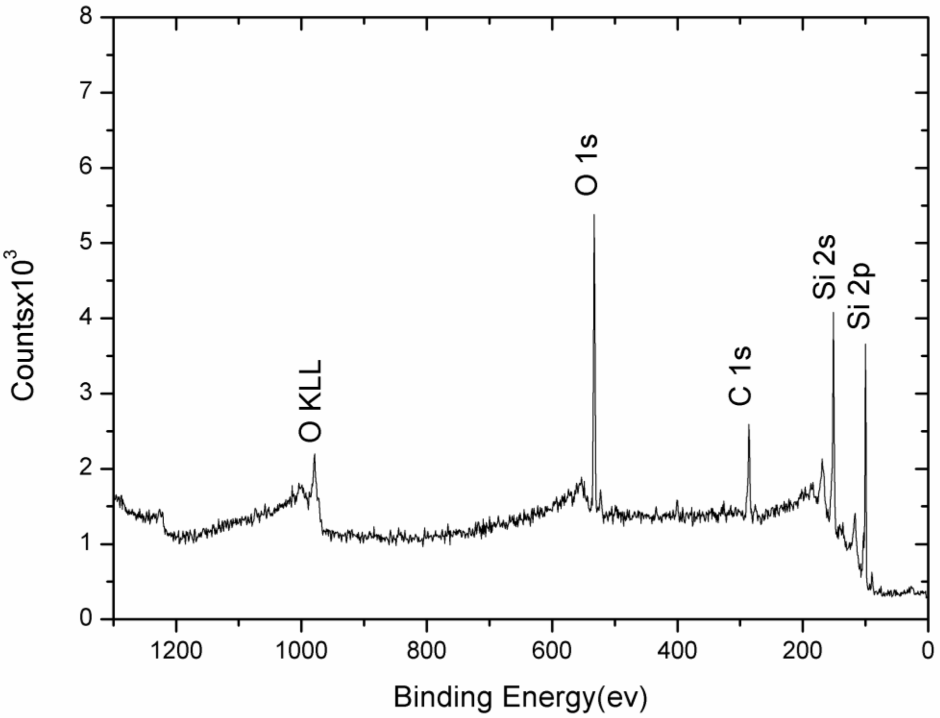

Figure 5.5 A widespread XPS spectrum of p-type Si crystal

In figure 5.5, as it is clear in XPS spectrum of the Si crystal has a sign for oxidation and for comprising Carbon atoms till some extent. Oxidation of Si and also of porous Si is a familiar situation for these sorts of studies with Silicon. The result is consistent with the oxidation study of porous silicon with XPS [114]. Hence, C is present but Si 2s, Si 2p, O1s and O KLL Auger are the most acute in the spectrum.

XPS results for other conditions such as PF2, RF2 and PF5 conditions used to obtain porous Si for various etching times is given below in figure 5.6, in figure 5.7 and in figure 5.8 respectively.

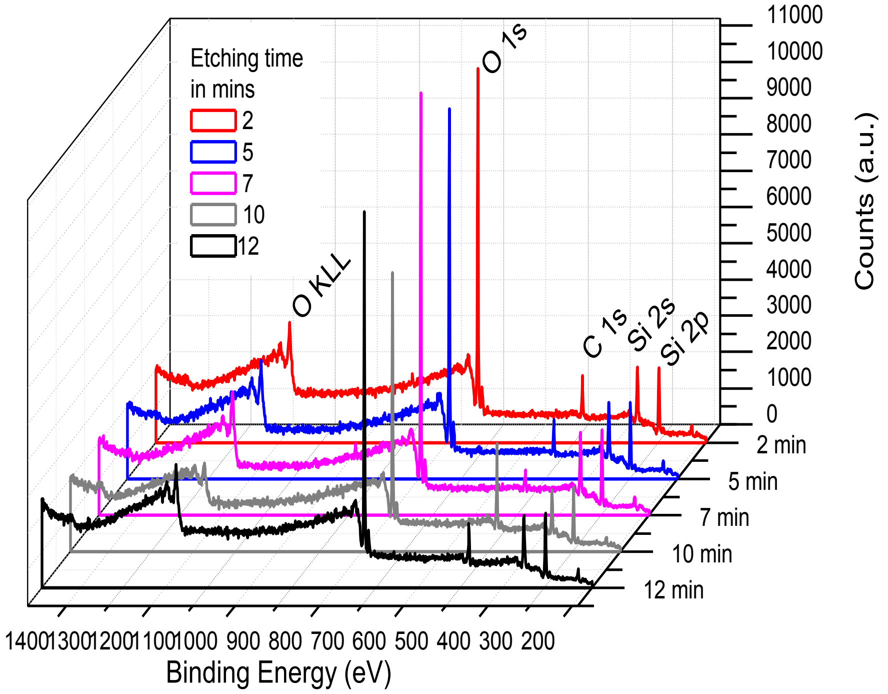

Figure 5.6 A widespread XPS spectrum of porous Si formed under PF2 condition

In figure 5.6, porous Si created under PF2 condition has similar appearance of peaks like the p type Si crystal does have. The increase in mainly O 1s peak and O KLL Auger is due to large surface to volume ratio and formation of pore structure and decrease in Si 2s and Si 2p because of etching process. In addition, the height of nanopillars can be predicted due to the amplitude of O 1s peaks. Because, all samples has been kept under ambient air for the same time at room temperature. So, the oxidation due to exposing surface of the samples with ambient air should have the same characteristics for the same sample. For PF2 condition, the amplitude of peaks given in figure can be put in order from the maximum to the minimum amplitude of O 1s as 7 min>12 min>4 min>2 min >10 min. Hence, this gives us an idea about the volume (abbreviated as V) of the pores in total (either nanopores or mesopores) might be sequenced as V (7 min)>V (12 min)>V (4 min)>V (2 min) >V (10 min).

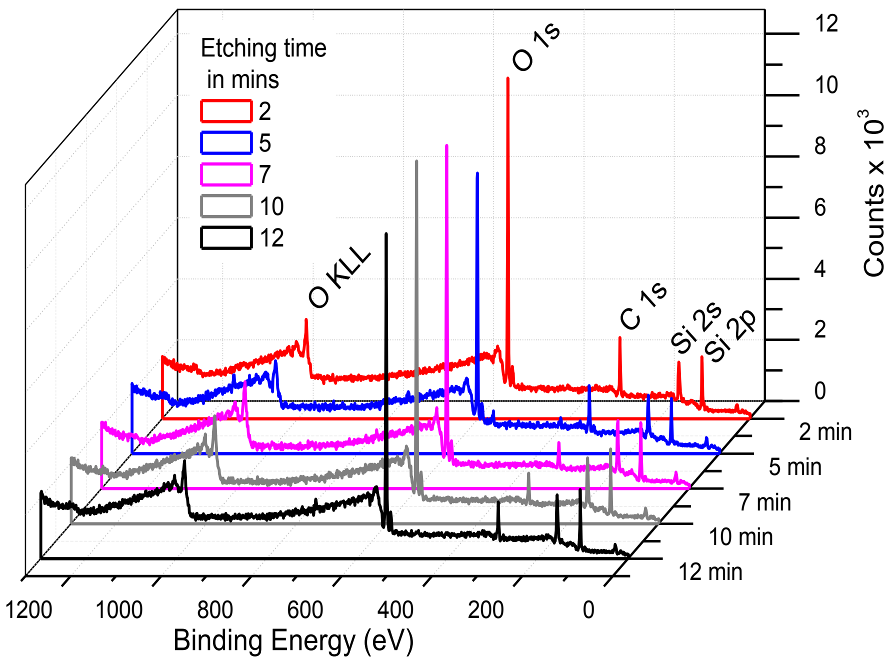

Figure 5.7 A widespread XPS spectrum of porous Si formed under RF2 condition

The peaks of O 1s, O KLL, Si 2p and of Si 2s Auger for porous Si formed by using RF2 conditions shown in figure 5.7 are similar to the peaks of those of PF2. The photo-electron emission amplitude of oxide peaks is given from the highest peak to the lowest one and sequenced as 10 min> 7 min>2 min>12 min >5 min. Except etching process during the 5 minutes, the etching process from 2 minutes to 10 minutes, the oxidation increases. So, it might be said that the volume of the pores of PS etched during 10 minutes is greater than those of the pores of PS for the etching time of 2 minutes, 5 minutes, 7 minutes and 12 minutes. On the other hand, for the etching time of 12 minutes, there is a decline in the height of the porous structure because there is a decrease in the emission of photoelectron of O 1s peak with respect to the peak value of etching time of 10 minutes. The physics behind this idea is that the samples having the etching time of 10 minutes and 12 minutes have been kept under same condition like exposing the prototypes with oxidation. Hence, it might be said that the amount of oxidation peak for XPS measurement is dependent on how high the nanopillar is.

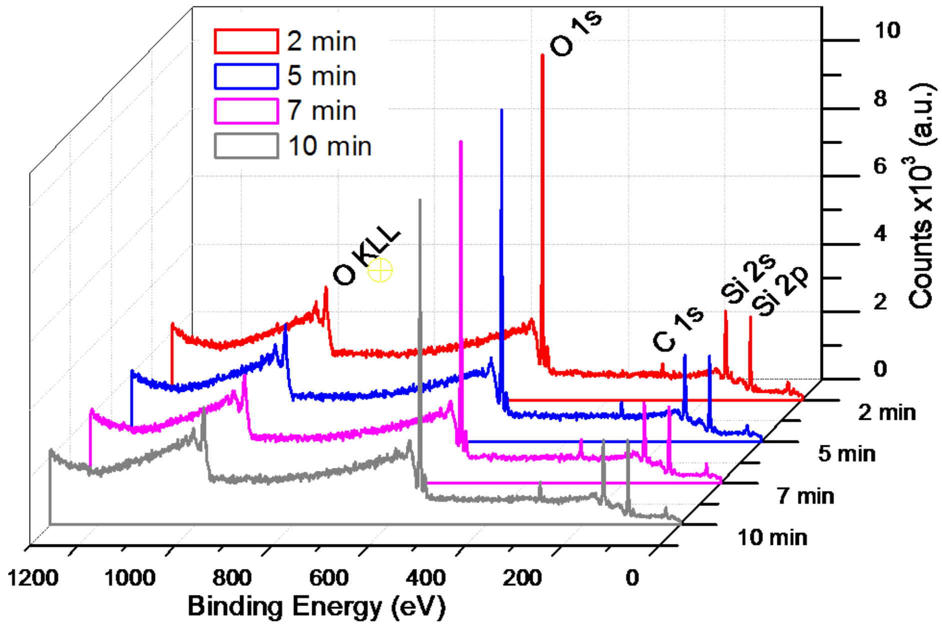

Figure 5.8 A widespread XPS spectrum of porous Si formed under PF5 condition

In figure 5.8, porous Si formed under PF5 condition represents that there is not so much change with O and Si peaks but decrease in C 1s peak. The reason for that is the increase of surfactant concentration. PF surfactant contains Benzene ring which contains C atoms and this will increase the interaction between surfactant and the surface of material. However, the oxidation of the prototypes formed under various etching times can be classified from the maximum count through the minimum count as 2 min>7 min>5 min>10 min. For this, it might be said that the etching process is maximum during 2 minutes; however, from PL results for etching times of 2 minutes of PF5 condition gives that there is no nanopore formation initiated. The pores which filled up with oxygen are mesopores which are not luminescent. On the other hand, due to increase in the O 1s peak, the etching process is more effective and the formed PS has more capacity to fill up with oxygen by increasing the etching time from 5 minutes to 10 minutes.

5.4 Confocal Microscope (CLSM) Results

The discovery that porous silicon luminescence at room temperature in the visible has prompted many research groups to produce a variety of light emitting porous silicon (LEPSi) specimens using several different fabrication techniques. Current research efforts study both LEPSi materials and devices.

The graphs of the mean intensity versus depth of LEPSi have been studied and presented below in figure 5.9, in figure 5.10 and in figure 5.11 according to various etching times for the same condition, and in figure 5.12, in figure 5.13, in figure 5.14, in figure 5.15, and in figure 5.16 according to the type of conditions such as RF2, PF2 and PF5 for the same etching time.

Figure 5.9 represents how mean intensity of photoluminescence changes with respect to depth of porosity of porous silicon which has been obtained under RF2 condition for various etching times.

Increasing the etching time makes an increase in the number of nanopillars on the surface and it is maximum for the etching time of 10 minutes in this study; however, it starts decreasing after this point.

On the sample etched during 2 minutes , has a constant intensity (namely pore size distribution is constant) at the beginning till 1.5 μm which is the point it diminishes and vanishes at the end of 3 μm.

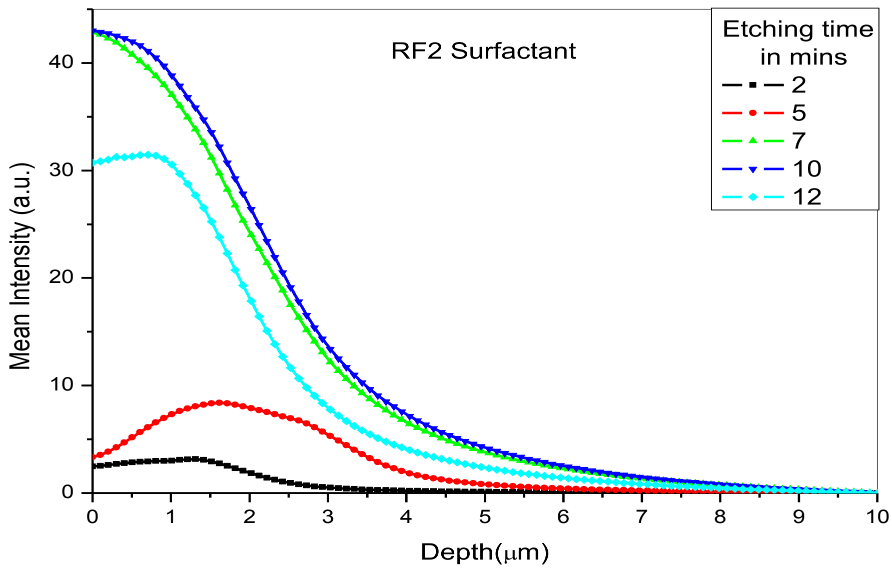

Figure 5.9 Mean Intensity versus depth of LEPSi formed under RF2 condition for various etching time

The prototype formed at the end of etching time of 5 minutes has a gausian-like- curve which has a maximum intensity at 1.8 μm where the number of nanopores is maximum. The intensity disappears after reaching 5.5 μm depth which states that the number of luminescent pores declines from 1.8 μm through 5.5 μm depth.

For the samples which have the etching times of 7 minutes and 10 minutes have a similar characteristics. The porosity is the maximum on the surface and it goes to zero exponentially.

The intensity of the sample for etching time of 12 minutes is constant until 1 μm. This means that radii of the pores are almost same till 1 μm depth which is the point it begins decreasing exponentially like the etching time of 7 minutes and 12 minutes.

Figure 5.10 states the mean intensity versus the depth of porosity of the PS which has been obtained under PF2 condition for different etching times.

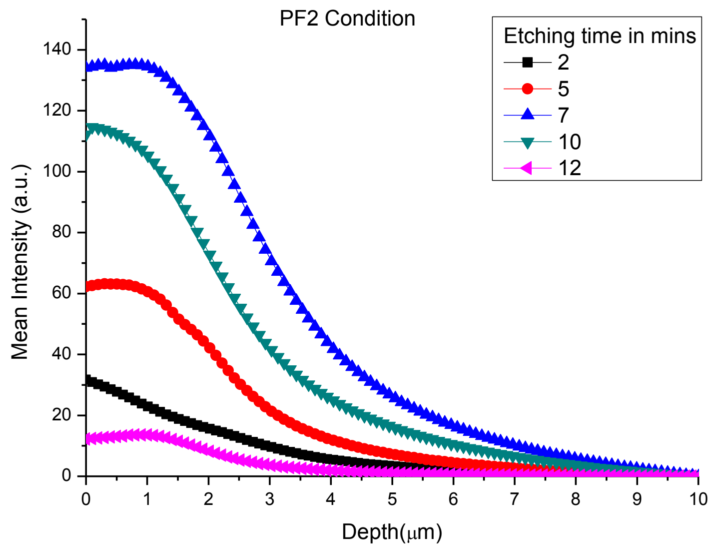

Figure 5.10 Mean Intensity versus Depth of LEPSi formed under PF2 condition for various etching time

It is seen that the samples formed under various etching time has maximum porosity on the surface. It is obvious that the intensity arises till the etching time of 7 mins and after that, it is observed that the intensity is getting decreased.

For the etching time of 5 mins, the PL intensity has no change which means the number of nanopillars is so close the each other. On the other hand, it starts decreasing the intensity exponentially after 1.5 μm depth. The contribution from luminescent pores goes on until 5 μm where intensity approaches to zero and ends. For etching times of 7 and 10 mins intensity is almost constant until 0.9 μm due to the fact that the maximum numbers of nanopillars are found between 0 (i.e. surface) and 0.9 μm distance. After this depth, the intensity due to the contribution from the numbers of nanopillars begins diminishing and ceases completely at the end of 10 μm.

For etching time of 12 mins , some layer are lifted off or etching away and some layers are at the start of the formation of porous structure just after peeled-off. This is because the intensity increases a little after 0.6 μm and starts decreasing 1 μm depth, meaning that first peeled off and then start etching again for the formation of porous layer.

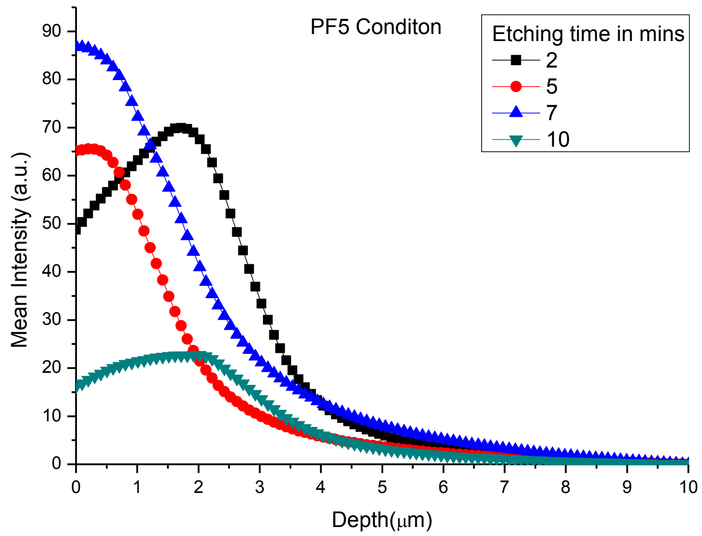

Figure 5.11 Mean Intensity versus Depth of LEPSi formed under PF5 condition for various etching time

In figure 5.11 the mean intensity versus depth of the sample is given for different duration of etching time. For increasing etching time such as 2, 5 and 7 mins, the number of the luminescent pores increases . For instance , the number of pores of the sample formed during etching time of 2 mins increases till 2 μm so the intensity increases as well. However , after this layer it starts decreasing.

For etching times of 5 and 7 mins, the intensity of samples diminishes exponentially. In other words , the number of luminescent pores decrease.

For etching time of the 10 mins , the intensity decreases and vanishes due to the fact that the nanowires gets thinner throughout the deeper layers of PS.

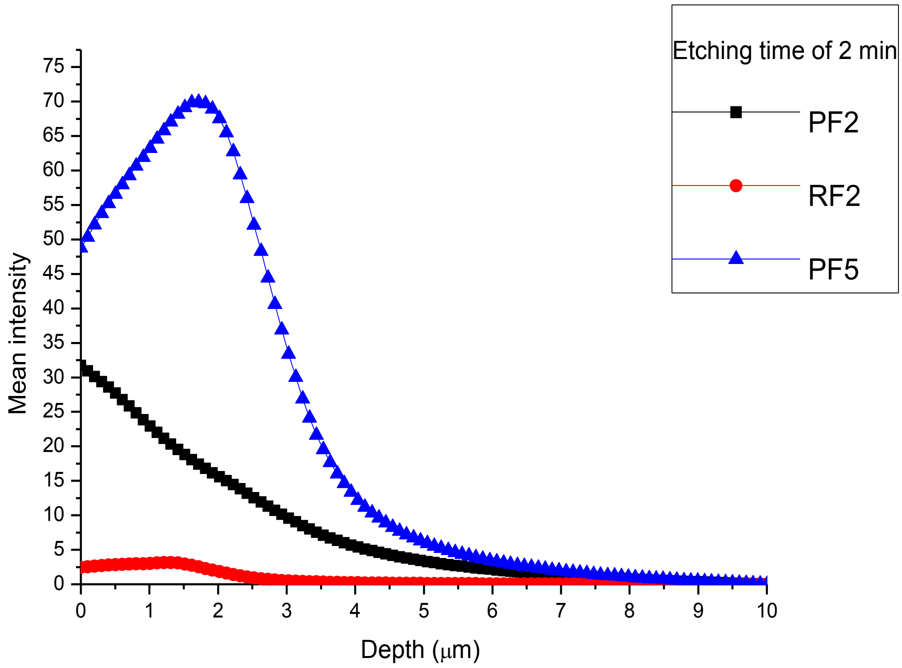

Figure 5.12 Mean Intensity versus Depth of LEPSi prototypes produced by PF2, RF2 and PF5 conditions for the etching times 2 minutes.

The samples formed under various conditions such as RF2, PF2 and PF5 during the etching time of 2 minutes have been compared in figure 5.12. The number of nanopores on the surface reaches the upper limit with respect to the other two conditions because mean intensity for PF5 is maximum compared to RF2 and PF2.

The luminescent contribution of RF2 ends at 3 μm depth so this condition etches less than the others during the 2 minutes etching time.

For the sample produced by PF2 and PF5 conditions for the etching time of 2 minutes, at first, the mean intensity inclines by increasing the concentration of surfactant till 2 μm and then decreases exponentially. The intensity of PSi formed with PF5 surfactant is larger than that of PSi created with PF2, because increasing the concentration of surfactant causes a gain in the number of nanopillars.

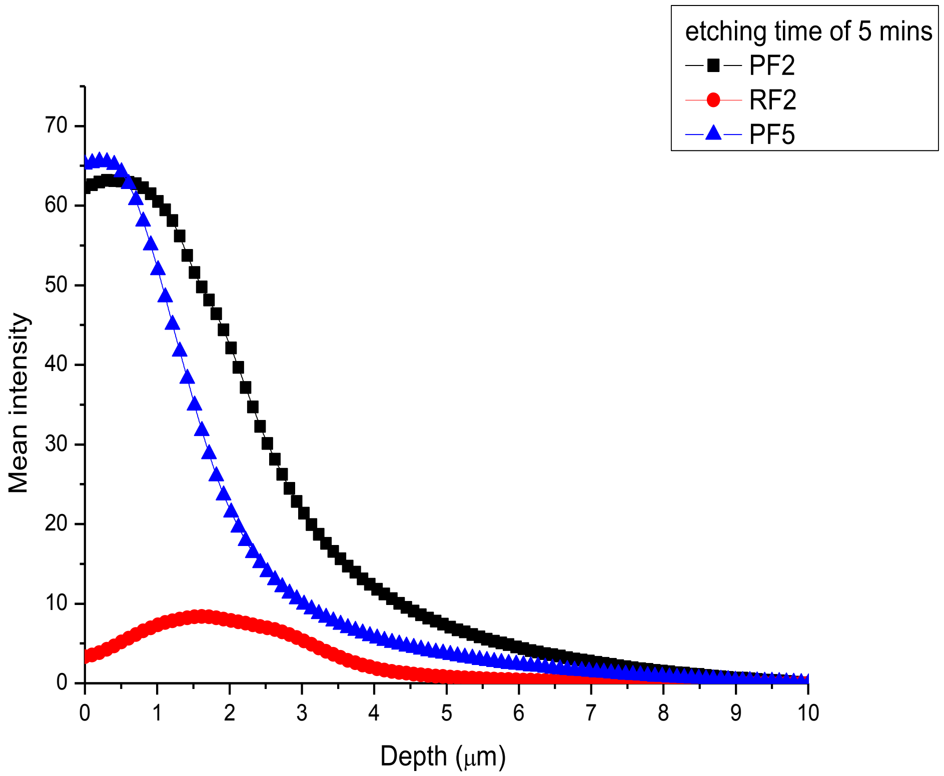

Figure 5.13 Mean Intensity versus Depth of LEPSi prototypes produced by PF2, RF2 and PF5 conditions for the etching times 5 minutes

In figure 5.13, it is given that the prototype produced under RF2 condition has a Gaussian-like curve; however, both of PF2 and PF5 conditions have a curve decreasing exponentially. It is observed that the PF condition affects more on the surface and throughout the deeper side of the sample than RF condition does. Because the mean intensity ends at 6 μm, on the other hand, the mean intensity approaches to zero at 10 μm for PF condition. Moreover, addition of surfactant concentration makes an increment in the number of nanopillars on the surface, nevertheless, the homogeneity decreases. In other words, PSi formed with PF2 has a constant intensity until 1.5 μm but PSi produced by PF5 condition has an invariable intensity till 0.7 μm.

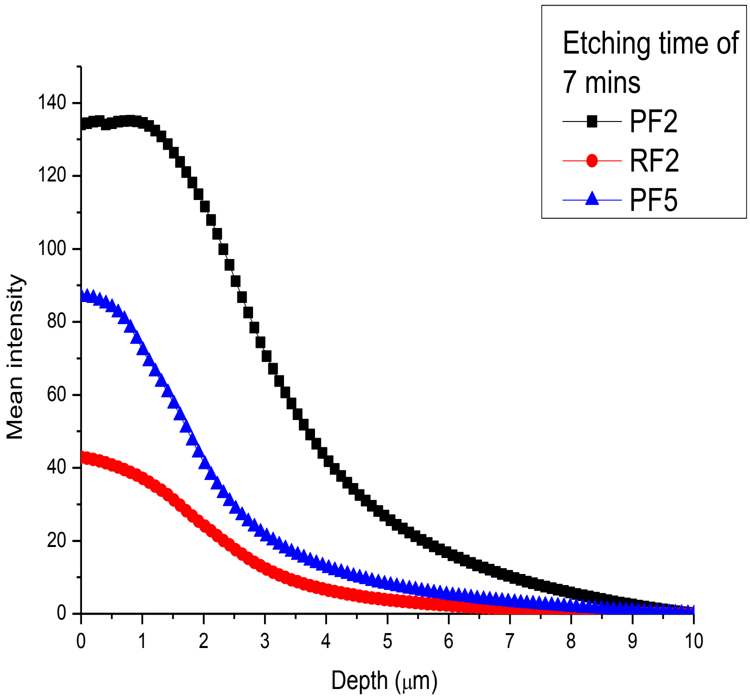

Figure 5.14 Mean Intensity versus Depth of LEPSi prototypes produced by PF2, RF2 and PF5 conditions for the etching times 7 minutes

For the etching time of 7 minutes, figure 5.14 represents that the prototypes obtained under RF2 conditions have similar characteristics of intensity which is maximum on the surface. For the three prototypes, it is observed that the PSi cross-sectional depth for the etching time of 7 minutes increases compared to the prototypes for the etching time of 2 and 5 minutes. In addition, the maximum porosity is found in the prototype formed with PF2 condition.

The increase in surfactant concentration from PF2 to PF5 makes a decline in the number of luminescent pores. The intensity for the sample made by PF2 condition represents a constant characteristic till 2 μm but the intensity of the sample created under PF5 starts decreasing intensity after 0.4 μm.

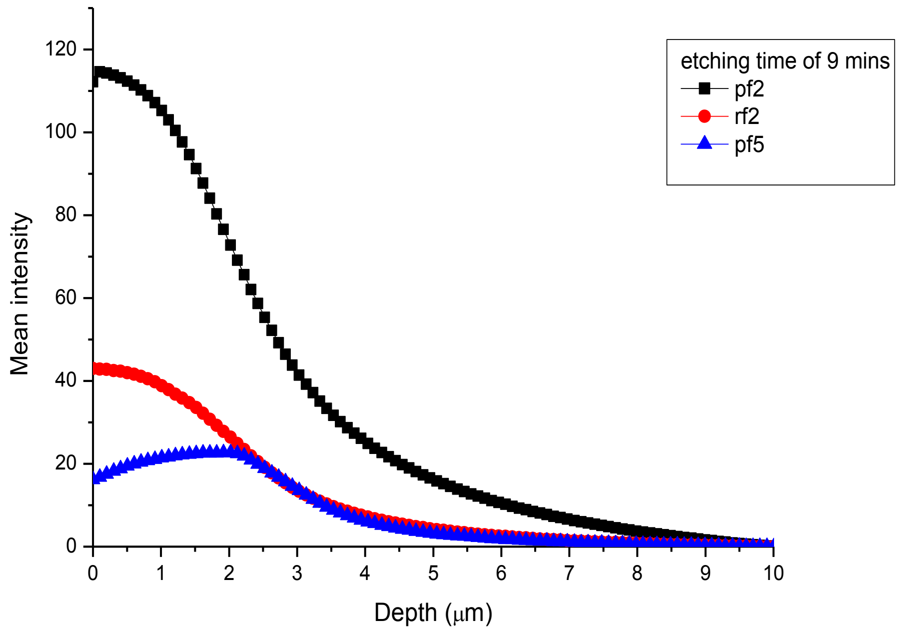

Figure 5.15 Mean Intensity versus Depth of LEPSi prototypes produced by PF2, RF2 and PF5 conditions for the etching times 10 minutes

As it is shown in figure 5.15, the prototypes made under RF2 and PF5 conditions have different characteristics in terms porosity and PSi depth until 2.2 μm. After this point, the PL intensity of the prototypes is getting closer to one another so this means the number of pores is almost same after 2 μm.

For PF2 condition, the intensity has a dissimilar behavior than those of RF2 and PF5 conditions. It seems that the intensity is the maximum on the surface and decreases exponentially with respect to depth of the sample.

By increasing the concentration of surfactant from PF2 to PF5, the intensity decreases. For PF2 condition, the donation of luminescent pores continues until 8 μm; however, it ends up at 6 μm for PF5 condition.

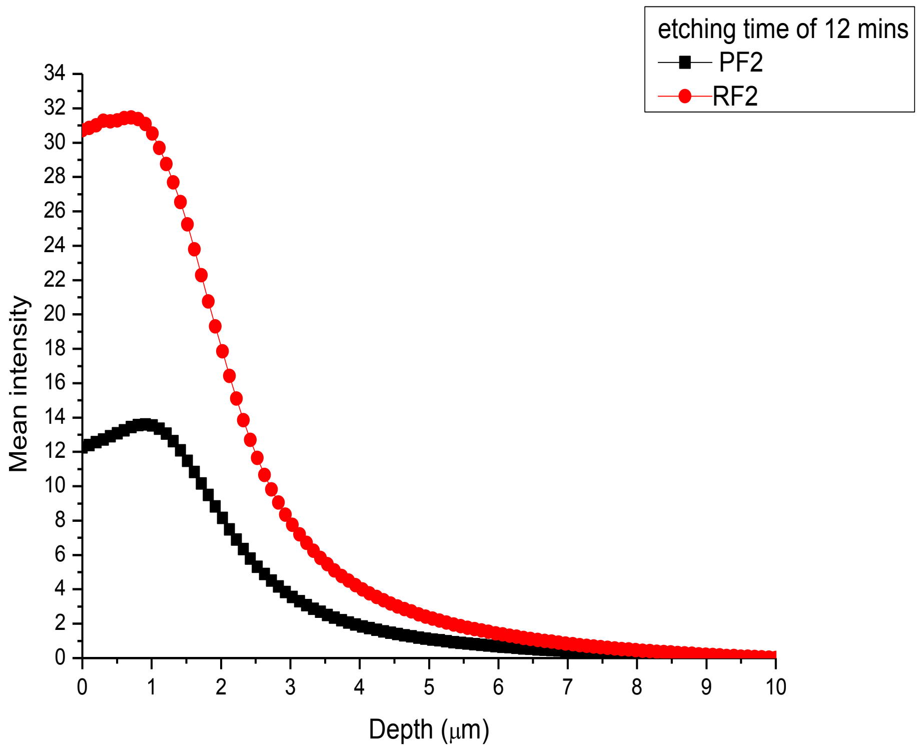

Figure 5.16 Mean Intensity versus Depth of LEPSi prototypes produced by PF2 and RF2 conditions for the etching times 12 minutes

In figure 5.16 for the etching time of 12 minutes, having higher intensity for the sample obtained under RF2 condition than those for the PF2 condition shows that RF2 condition is more effective for decreasing the surface tension and supply the solution penetrating towards the deeper side of the layers of the wafer. The number of nanopillars is much larger with RF2 condition than those of PSi produced by PF2 condition.

Another important comparison between RF2 and PF2 conditions is that despite the amount of nanopillars are different; the depth distance is 7 μm which is the same for the prototypes created under RF2 and PF2 conditions.

CHAPTER 6

CONCLUSION

In this study, the characteristics of the room temperature photoluminescent porous Si obtained by using two different surfactants have been investigated with techniques called PL, PLE, XPS and Confocal Microscopy. The samples were prepared from Boron doped (100) Si wafers which has 525 μm thickness and >1 ohm.cm resistivity by using standard stain etching procedure with the addition of various surfactants which is called and used in the thesis study as PF and RF.

First of all, the excitation wavelength of porous Si has been obtained by using photoluminescence excitation spectrometry. It is found that the prototypes of porous Si have excitation wavelength changing from 345 nm to 350 nm. Secondly, PL results give the relationship between PL intensity and its wavelength or energy. In a report [57], the porosity is directly proportional to the intensity of PL. If the PL intensity of PSi formed under RF2 condition is compared to that of PSi created under both PF2 and PF5 conditions, the peak value of RF2 is much higher than that of PF. Hence, the porosity of PSi film obtained by using RF2 condition must be greater than that of PSi formed by using PF conditions.

On the other hand, the change in band gap is related to decrease in nanocrystallite size is given in figure 2.6(a) for PF2 and RF2 conditions and also in figure 2.6 (b) for PF5 condition. Former results have been given theoretically [57] and experimentally [58,59].

The emission wavelengths of PSi in this study are found to be around 620 ± 1 nm for RF2 condition , 617 ± 1 nm and 621 nm for PF2 condition , both 617 ± 1 and 626 ± 1 nm for PF5 condition in visible region of electromagnetic spectrum.

The band gap energies for each RF4, PF4 and PF5 conditions are equal to the corresponding energy values of emission wavelength which are given respectively as 2.007±0.003 eV, both of 2.014±0.003 eV and 2.014 nm, both 2.013±0.003 eV and 1.984±0.003 eV. The band gap energy graphs estimate the nanopore sizes such as 2.600 ± 0.005nm, both of 2.570 ± 0.005nm and 2.560± 0.005 nm, and both 3.020±0.005 nm, 2.960± 0.005nm for PS formed via RF2, PF2 and PF5 respectively.

From XPS results, the surface analysis of PS prepared with the surfactants of RF2, PF2, and PF5 have been investigated. The amount of oxidation with respect to etching time has been compared with the formation of PSi under the various conditions of surfactants. As the size of quantum wire or nanocrystallite decreases, the energy band gap of the nanocrystallite increases. In other words, there is a loss of the energy of emitted photon due to the quantum confinement effect which is the radiative recombination of a free exciton, i.e. an electron-hole pair.

At last, confocal microscopy results have given the information about the intensity of the photoluminescence and the depth of PSi relationship. The microscopy result is informative that how the depth profile of PSi can be adjusted by the etching time for the addition of the same amount of the surfactant. For example, at the end of the etching time of 2 minutes under PF2 condition as shown in figure 5.10, the height of nanopillars is 4 μm on the other hand the height of the nanopillars has a value of 10 μm for the etching time of 7 minutes under PF2 condition. Moreover, the confocal microscopy results give an idea about how the surfactant type is effective on the depth of PSi. By changing the amount and type of surfactant type for the same etching time, the depth profile can be tunable. For instance as represented in figure 5.14, the intensity versus depth profile graph of PSi for the etching time of 7 minutes under RF2, PF2 and PF5 conditions almost has the same depth value as 10 μm.

These results are supportive and effective till some degree for formation of porous Si. Some characteristic behaviors are said to be supported by some other tools related to surface studies like SEM, Auger Spectroscopy, XRD and so on.

REFERENCES

[1] Volker Lehmann, *Electrochemistry of Silicon: Instrumentation, Science, Materials and Applications,* pp.1, (2002)

[2] A. Güntherschulze, H. Betz, *Electrolytkondensatoren (Ed. M. Krayn),* Techn. Verlag H. Cram, Berlin, (1937)

[3] P. F. Schmidt, J. Orashnik, C. C.Hardman, *Solid-State Electron*, 7, pp. 631, (1964)

[4] P. F. Schmidt, W. Michel, J. *Electrochem. Soc.,* 104, pp. 230–236, (1957)

[5] R. Memming, G. Schwandt, *Surf.Sci.*, 4, pp. 109, (1966)

[6] M. J. J. Theunissen, J. A. Appels, W.H. C. G. Verkuylen, *J. Electrochem.Soc*., 117, pp. 959–965, (1970)

[7] H. J. A. van Dijk, J. de Jonge, *J. Electrochem. Soc.*, 117, pp. 553–554, (1970)

[8] A. L. Dalisa, W. K. Zwicker, D. J.DeBitetto, P. Harnack, *J. Appl. Phys.* 17, pp. 208–210, (1970)

[9] Y. Watanabe, T. Sakai, *Rev. Electron.Commun. Labs*, 19, pp. 899, (1971)

[10] M. J. J. Theunissen, *J. Electrochem. Soc*., 119, pp. 351–360, (1972)

[11] V. Lehmann, H. Föll, *J. Electrochem. Soc.,* 135, pp. 2831–2835, (1988)

[12] G. Bomchil, R. Herino, K. Barla, J.C. Pfister, *J. Electrochem. Soc*., 130, pp. 1611–1614, (1983)

[13] Y. Arita, J. Cryst. *Growth*, 45, pp. 383–392, (1978)

[14] T. Unagami, *Jpn. J. Appl. Phys.,* 2, pp. 231–241, (1980)

[15] R. P. Holmstrom, J. Y. Chi, *Appl. Phys. Lett*., 42, pp. 386–388, (1983)

[16] K. Imai, H. Unno, *IEEE Trans. ElectronDevices*, ED-31, pp. 297–302, (1984)

[17] T. L. Lin, S. C. Chen, Y. C. Kao, K. L.Wang, *J. Appl. Phys*., 48, pp. 1793, (1986)

[18] C. Pickering, M. I. J. Beale, D. J.Robbins, P. J. Pearson, R.Greef, *J. Phys. C: Solid State Phys*., 17 pp. 6535–6552, (1984)

[19] L. T. Canham, *Appl. Phys. Lett*., 57, pp. 1046–1048, (1990)

[20] V. Lehmann, U. Gösele, *Appl. Phys.Lett*., 58, pp. 856–858, (1991)

[21] V. Lehmann, H. Cerva, U. Gösele, *Mater. Res. Soc. Symp. Proc*., 256, pp. 3–6, (1992)

[22] T. Ito, T. Ohta, O. Arakaki, A. Hiraki, *Mater. Res. Soc. Symp. Proc*., 256, pp. 127, (1992)

[23] A. G. Cullis, L. T. Canham, P. D. J.Calcott, *J. Appl. Phys*., 82, pp. 909–965, (1997)

[24] W. Theiß, *Surf. Sci. Rep*., 29, pp. 91–192, (1997)

[25] Jan G. Korvink and Andreas Greiner , *Semiconductors for Micro and Nanotechnology—An Introduction for Engineers*, Wiley-VCH Verlag GmbH, Weinheim , pp.33 , (2002)

[26] R. W. Cahn, P. Haasen, E.J. Kramer, *Materials Science and Technology*, 4, (1991)

[27] Jasprit Singht , *Semiconductor Devices: Basic Principles* , John-Wiley , (2001)

[28] E. F. Schubert , *Doping in III-V Semiconductors* ,Cambridge Studies in Semiconductor Physics and Microelectronic Engineering, AT&T , pp.107-118 , (1993)

[29] T.E. Jenkins, *Semiconductor Science*, Prentice Hall, New York 1st Ed., pp. 74 and 175-177, (1995)

[30] B. Ünal, "*Optical, Electrical And Structural Properties Of Nanostructured Silicon And Silicon-Germanium Alloys"*, Ph. D. Thesis, De Montfort University of Leicester Press, (1998)

[31] Sasan Fathpour , Fundamental of Optical Science Lecture Notes ,(2008)

[32] L.T. Canham, *Materials Research Society,PA* pp. 175-178, (1992)

[33] (a) J.C. Vial and J. Derrien, *Porous Silicon Science and Technology*, *Lect. 2,* pp. 17-32, (1994)

(b) R. Memning and G. Schwandt, *Surf. Sci*., 4, pp. 109, (1966)

[34] V. Lehmann and U. Gösele, *Appl. Phys. Lett.*, 58, pp. 856, (1991)

[35] H. Gerischer, P. Allongue and V. Costan Kieling, Ber. Bunsenges, *Phys. Chem*., 97 pp. 753, (1993)

[36] P.C. Searson and X.G. Zhang, *J. Electrochem. Soc.,* 137, pp. 2539, (1990)

[37] F. Ozanam, J.-N. Chazalviel, A. Radi and M. Etman, *J. Electrochem. Soc.*, 139, pp. 2491, (1992)

[38] V. Lehmann and U. Gösele, *Adv. Mater,* 4, pp. 114, (1992)

[39] V. Lehmann and H. Foll , *J. of Electrochem*, 137, pp. 653, (1990)

[40] V.M. Dubin, *Surf. Sci*. 274, pp. 82, (1992)

[41] (a) P.C. Searson, J.M. Macaulay and F.M. Ross, *J. Appl. Phys.*, 72, pp. 253, (1992)

(b) T. Oguro, H. Koyama, T. Ozaki, N. Koshida, *J. Appl. Phys.* 81, pp. 1407, (1997)

[42] (a) V. Lehmann, H Cerva and U. Gosele, *MRS. Proc*., 256, pp. 3, (1992)

(b) V. Lehmann and H. Foll, *J. of Electrochem*, 137, pp. 653, (1990)

[43] Y. Kang and J. Jorne, *Appl. Phys. Lett.*, 62, pp. 2224, (1993)

[44] L.T. Canham, *Appl. Phys. Lett.,* 57, pp. 1046, (1990)

[45] C. Delure, G. Allan and M. Lannoo, *Phys. Rev. B.,* 48, pp. 11024, (1993)

[46] P.D.J. Calcott, K.J. Nash, L.T. Canham, M.J. Kane and D. Brumhead, *J. Phys: Condens. Matter.,* 5L91, (1993)

[47] B. K. Meyer, D.M. Hofmann, W. Stadler, V.Petrova-Koch, F. Koch, P. Omling and P. Emanuelsson, *Appl. Phys. Lett.*, 63, pp. 2120, (1993)

[48] J. P. Proot, C. Delerue, G. Allan, *Appl. Phys. Lett.*, 61, pp. 1948, (1992)

[49] C. Delerue, M. Lannoo, G. Allan, E. Martin, *Thin Solid Films*, 255, pp. 27, (1995)

[50] S.Y. Ren and J.D. Dow, *Phys. Rev. B,* 45, pp. 6492, (1992)

[51] M. Lannoo, C. Delerue, G. Allan and E. Martin, *MRS Proc.*, 258, pp. 13, (1995)

[52] N. A. Hill, K. B. Whaley *J. Electron. Mat.*, 25, pp. 269,(1996)

[53] D. J. Lockwood, *Solid State Commun.*, 92, pp. 101, (1994)

[54] (a) J..P. Proot, C. Delerue, G. Allan, *Appl. Phys. Lett*., 61, pp. 1948, (1992)

(b) A. G. Cullis, L.T. Canham, G.M. Williams, P.W Smiths and O.D. Dosser, *J. Appl. Phys*., 75, pp. 493, (1994)

[55] S.Gardelis, U. Bangert, and B. Hamilton, *Thin Solid Films*, 255, pp. 167, (1995)

[56] Guozhong Cao , *Nanostructures & Nanomaterials* , İmperial College Press , (2004)

[57] L. Wang and A. Zunger, *J. Phys. Chem.* 98, pp. 2158, (1994)

[58] J.von. Behren , T.van Buuren , M. Zacharias , E. H. Chimowitz , and P.M. Fauchet, *Solid State Commun.*, 105, pp. 317, (1998)

[59] Q.Zhang and S.C.Bayliss, *J.Appl. Phys.* 79, pp. 1351, (1996)

[60] C. Colvard, *in Encyclopedia of Materials Characterization*, C.R. Brundle,

C.A. Evans Jr., and S. Wilson, Buttenvorth-Heinemann, Stoneham, MA, pp. 373, (1992)

[61] C.R. Kagan, C.B. Murray, and M.G. Bawendi, *Phys*. Rev. B54, pp.8633 , (1996).

[62] Al. L. Efros and M. Rosen, *Ann. Rev. Matev. Sci*. 30, pp.475 , (2000)

[63] A.I. Ekimov and A.A. Onushchenko, *Sov. Phys. - Semicond*. 16 , pp.775 , (1982)

[64] R. Rossetti, S. Nakahara, and L.E. Brus, *J. Chem. Phys*. , 79, pp.1086 , (1983)

[65] A.P. Alivisatos, *J. Phys. Chem.* , 100 , pp.13226 , (1996)

[66] M.L. Chen, M.Y. Chou, W.D. Knight, andW.A. deHeer, *JIPhys. Chem.* , 91 , pp.3141, (1987)

[67] C.R.C. Wang, S. Pollack, T.A. Dahlseid, G.M. Koretsky, and M. Kappes, *J.Chem. Phys.* , 96, pp.7931 , (1992)

[68] A.J. Nozik and R. Memming, *J. Phys. Chem.* , 100 , pp.13061 , (1996)

[69] A.P. Alivisatos, *J. Phys. Chem.* , 100, pp.13226 , (1996)

[70] Y. Wang and N. Herron, *J. Phys. Chem.* , 95, pp. 525 , (1991)

[71] L.E. Brus, *Appl. Phys.* A53, pp.465 , (1991)

[72] C.H. Perry, F. Lu, F. Namavar, N.M.Kalkhoran, and R.A. Soref, *MRS Proc.*, 256 pp.153, (1992)

[73] (a) P.D.J. Calcott, Materials Sci. and Eng. B- Solid State Materials For Advanced Technology B51, pp. 132–140, (1998)

(b) M. Fuji, S. Hayashi and K. Yamamoto, *Appl. Phys. Lett.*, 73, pp. 3108, (1998)

[74] I. Mihalcescu, M. Ligeon, F. Muller, R. Romestain and J.-C. Vial, J. Lumin, 57, pp.111, (1993)

[75] J.L. Gole, D.A. Dixon, *Phys. Rev. B- Conden. Matt.*, 57, pp. 12002, (1998)

[76] C. Delerue, *Phys. Rev. B*, 48, pp.11024, (1993)

[77] P.Deak, *Phys. Rev. Lett.*, 69, pp. 2531, (1992)

[78] X.Y. Hou, g. Shi, W. Wang, F.L. Zhang, P.H. Hao, D.M. Huang and X. Wang, *Appl. Phys. Lett.*, 62, pp. 1097, (1993)

[79] P. Basmaji, *MRS Proc.*, 283, pp.227, (1993)

[80] D.J. Lockwood, A. Wang, B.Bryskiewicz, *Solid State Commun.*, 89, pp. 587, (1994)

[81] D.J. Lockwood, *Solid State Comm.*, 92, pp.101, (1994)

[82] K. Murayama, S. Miyazakiand , M. Hirose, *Jpn. J. Appl. Phys*., 31, pp. 1358, (1992)

[83] T. Matsumoto, N. Hasegawa, T. Tamaki, K. Ueda, T. Futagi, H. Mimura, Y. Kanemitsu, *Jpn. J. Appl.Phys*., 33, pp. 35, (1994)

[84] J. Oswald, J. Pastrnak, A. Hospodkova and J. Pangrac, *Solid State Commun*., 89, pp. 297, (1994)

[85] V. Petrovakoch, T. Muschik, A. Kux, B.K. Meyer, F. Koch and V. Lehmann, *Appl Phys Lett.*, 61, pp. 943, (1992)

[86] E. Massone, A. Foucaran and J. Camassel, J Lumin., 57, pp. 51, (1993)

[87] Y. Suda, T. Ban, T. Koizumi, H. Koyama, Y. Tezuka, S. Shin, and N. Koshida, *Jpn. J. Appl. Phys*. 33, pp. 581, (1994)

[88] G. Di Francia, S. Turchini, T. Properi, F. Martelli, G. Amato and M. De Santis, *J. Appl. Phys.*, 76, pp. 3787, (1994)

[89] G. Amato, G. Di Francia, P. Menna, and D. Ninno, *Europhys Lett.*, 25, pp. 471, (1994)

[90] W. Kern and D. Puotinen, *RCA Review*, 31, pp. 187, (1970)

[91] Werner Kern, "Overview and Evolution of Semiconductor Wafer Contamination and Cleaning Technology," in "Handbook of Semiconductor Wafer Cleaning Technology: Science, Technology, and Applications," Werner Kern ed., Noyes Publications, (1993)

[92] Coffer JL., L. Canham , ‘‘Porous silicon formation by stain etching, in Properties of Porous Silicon’’ , Institution of Engineering and Technology, London, pp. 23-28 , (1997)

[93] L. Canham , *Properties of Porous Silicon*, The Ins. of Electrical Engineers Press, London, (1997)

[94] Baeurle SA, Kroener J ,"Modeling Effective Interactions of Micellar Aggregates of Ionic Surfactants with the Gauss-Core Potential". J. Math. Chem., 36 , pp.409–421 , (2004)

[95] D. Briggs , *Handbook of X-ray and ultraviolet photoelectron spectroscopy* , Heyden , pp.398 , (1977)

[96] M. Orhring, *The Materials Science of Thin Films*, Academic Press, (1992)

[97] Lu, Peter J. , " Confocal Scanning Optical Microscopy and Nanotechnology " , *Handbook of Microscopy for Nanotechnology*, New York: Kluwer , pp. 3-24, (2005)

[98] Denis Semwogerere , Eric R. Weeks , *Encyclopedia of Biomaterials and Biomedical Engineering* , Taylor & Francis, (2005)

[99] Sheppard, C.J.R.; Shotton, D.M. Introduction. *In Confocal Laser Scanning Microscopy*; Springer-Verlag New York Inc.: New York, pp.1–13 , (1997)

[100] S.C. Bayliss, P. Anstee, D.A. Hutt, Q. Zhang, N. Danson, J. Bates and A. Waddilove. *J. Appl. Phys.* 76, pp. 5171, (1994)

[101] T.K. Sham, D.T. Jiang, I. Coulthdrd, J.W. Lorimer, X.H. Feng, K.H. Tan, S.P. Frigo, R.A. Rosenberg, D.C. Houghton and B. Bryskiewiez. *Nature*, 363, pp. 33, I (1993)

[102] G. Di Francis, S. Turchini, T. Prosperi, F. Martelli, G. Amato and M. De Santis, *J. Appl. Phys.* 76 pp. 3787, (1994)

[103] V. Bangert, S. Cardelis, B. Hamilton and R. Pettifer, *Phys. Status Solidi bl* 190, pp.69, (1995)

[104] L.C. Earwaker , J.P.G. Farr , I. Alexander , J.M. Sturland and J.M. Keen, *Nucl. Instr. Meth*. 218, pp. 381, (1993)

[105] H. Miinder. in: Jean-Claude Vial, Jacques Derrien, *Porous Silicon Science and Technology*, Springer-Verlag Publisher, Berlin, New York, Les Ulis, (1995)

[106] R.P. Vasquez, R.W. Fathauer, T. George. A. Ksendzov and T.L. Lin, *Appl. Phys. Lett*. 60, pp.1004, (1992)

[107] K. Murakoshi and K. Vosaki, *Appl. Phys. Lett*. 62, pp. 1676, (1993)

[108] N. Koshida and H. Koyama, *Mater. Res. Soc. Symp. Proc*. 283, pp. 337, (1993)

[109] S. Poulin, Y. Diawara. J.F. Currie, A. Yelon. S.C. Gujrdthi and V. Petrova Koch. *Mater. Res. Soc. Symp.* Proc. 283 pp. 83, (1993)

[110] H. Minder. M.G. Berger, S. Frohnhoff, M. Thonissen, H. Lith, M. Jeske and J.W. Schulze. J. Lumin. 57 pp. 223, (1993)

[111] M. Jeske, K.G. Jung. J.W. Schultze. M. Thiininsen and H. Miinder, Surf. Interf. Anal. 22 pp. 363 (1994) .

[112] A. Roy A. Chainani, D.D. Sarma and A.K. Sood. Appl. Phys. Lett. 61 pp. 1655 (1993)

[113] K. Inove, K. Maehashi and H. Nakashimd, Jpn. J. Appl. Phys. 32 pp.361, (1993).

[114] F. Leisenberger, R. Duschek, R. Czaputa, F.P. Netzer, G. Beamson, J.A.D. Matthew Applied Surface Science 108, pp. 273-281, (1997)